AMERICAN SOCIETY FOR MICROBIOLOGY | Journal of Virology®

VIRUS-CELL INTERACTIONS

The SETD2 Methyltransferase Supports Productive HPV31 Replication through the LEDGF/CtIP/Rad51 Pathway

Michelle Mac,[a] Brianna M. DeVico,[b] Sophia M. Raspanti,[b] Cary A. Moody[a,b]

[a]Department of Microbiology and Immunology, University of North Carolina at Chapel Hill, Chapel Hill, North Carolina, USA
[b]Lineberger Comprehensive Cancer Center, University of North Carolina at Chapel Hill, Chapel Hill, North Carolina, USA

ABSTRACT The human papillomavirus (HPV) life cycle takes place in the stratified epithelium, with the productive phase being activated by epithelial differentiation. The HPV genome is histone-associated, and the life cycle is epigenetically regulated, in part, by histone tail modifications that facilitate the recruitment of DNA repair factors that are required for viral replication. We previously showed that the SETD2 methyltransferase facilitates the productive replication of HPV31 through the trimethylation of H3K36 on viral chromatin. SETD2 regulates numerous cellular processes, including DNA repair via homologous recombination (HR) and alternative splicing, through the recruitment of various effectors to histone H3 lysine 36 trimethylation (H3K36me3). We previously demonstrated that the HR factor Rad51 is recruited to HPV31 genomes and is required for productive replication; however, the mechanism of Rad51 recruitment has not been defined. SET domain containing 2 (SETD2) promotes the HR repair of double-strand breaks (DSBs) in actively transcribed genes through the recruitment of carboxy-terminal binding protein (CtBP)-interacting protein (CtIP) to lens epithelium-derived growth factor (LEDGF)-bound H3K36me3, which promotes DNA end resection and thereby allows for the recruitment of Rad51 to damaged sites. In this study, we found that reducing H3K36me3 through the depletion of SETD2 or the overexpression of an H3.3K36M mutant leads to an increase in γH2AX, which is a marker of damage, on viral DNA upon epithelial differentiation. This is coincident with decreased Rad51 binding. Additionally, LEDGF and CtIP are bound to HPV DNA in a SETD2-dependent and H3K36me3-dependent manner, and they are required for productive replication. Furthermore, CtIP depletion increases DNA damage on viral DNA and blocks Rad51 recruitment upon differentiation. Overall, these studies indicate that H3K36me3 enrichment on transcriptionally active viral genes promotes the rapid repair of viral DNA upon differentiation through the LEDGF-CtIP-Rad51 axis.

IMPORTANCE The productive phase of the HPV life cycle is restricted to the differentiating cells of the stratified epithelium. The HPV genome is histone-associated and subject to epigenetic regulation, though the manner in which epigenetic modifications contribute to productive replication is largely undefined. In this study, we demonstrate that SETD2-mediated H3K36me3 on HPV31 chromatin promotes productive replication through the repair of damaged DNA. We show that SETD2 facilitates the recruitment of the homologous recombination repair factors CtIP and Rad51 to viral DNA through LEDGF binding to H3K36me3. CtIP is recruited to damaged viral DNA upon differentiation, and, in turn, recruits Rad51. This likely occurs through the end resection of double-strand breaks. SETD2 trimethylates H3K36me3 during transcription, and active transcription is necessary for Rad51 recruitment to viral DNA. We propose that the enrichment of SETD2-mediated H3K36me3 on transcriptionally active viral genes upon differentiation facilitates the repair of damaged viral DNA during the productive phase of the viral life cycle.

KEYWORDS CtIP, DNA replication, LEDGF, Rad51, SETD2, DNA damage, epigenetics, life cycle, papillomavirus

Editor Lori Frappier, University of Toronto

Address correspondence to Cary A. Moody, camoody@med.unc.edu.

The authors declare no conflict of interest.

Received 7 February 2023
Accepted 17 April 2023
Published 8 May 2023

Human papillomaviruses (HPVs) are small DNA viruses that exhibit a strict tropism for epithelial cells. Over 400 types of HPV have been identified that infect either the cutaneous or mucosal epithelium (1). Of the types that infect the genital mucosa, the low-risk HPV types (e.g., HPV6 and 11) induce benign genital warts, whereas the high-risk HPV types (e.g., HPV16, 18, 31, and 45) cause cervical carcinomas and are associated with other anogenital malignancies, such as penile, vulvar, and anal carcinomas. Additionally, the high-risk HPV types are associated with an increasing number of oropharyngeal carcinomas, predominantly HPV16 (2). While the prophylactic HPV vaccines are efficacious in preventing the development of cervical cancer, they are not therapeutic, and there are currently no antivirals to treat HPV-associated diseases. Cervical cancer remains the most frequent cause of cancer deaths in developing countries and in the United States (3). HPV-associated oropharyngeal carcinoma constitutes up to 90% of all new incidences of oropharyngeal cancers in recent years (4).

The life cycle of HPV is dependent on the differentiation status of host keratinocytes. HPV infects the basal cells of the stratified epithelium that are thought to become exposed through microlesions (5). Following infection, the HPV episomes transiently amplify to 50 to 100 copies per cell (6). Recent studies suggest that episomal maintenance in undifferentiated cells occurs through an amplification process, with the majority of viral genomes being lost upon cell division due to them being untethered from host chromosomes, essentially resetting the copy number to the pre-S phase level (7). The productive phase of the HPV life cycle is activated upon epithelial differentiation, which leads to the expression of late viral genes, the amplification of viral genomes to hundreds to thousands of copies per cell, and virion assembly and release from the uppermost layers of the epithelium (6, 8, 9). Whereas normal keratinocytes exit the cell cycle upon differentiation, the HPV E6 and E7 oncoproteins deregulate normal checkpoint controls to push infected cells back into the cell cycle upon differentiation, thereby creating an environment that is conducive to viral replication (10).

High-risk HPV E7 proteins contribute to the establishment of a replication-competent environment in differentiating cells, in part, through the activation of the ataxia-telangiectasia-mutated (ATM) and ATM and Rad3-related (ATR) DNA damage kinases, which respond to double-strand DNA breaks (DSBs) and single-strand DNA (ssDNA), respectively (10). High-risk HPVs use ATM and ATR signaling components to facilitate the high-fidelity replication and amplification of viral genomes upon differentiation (11–15). The HPV genome is histone-associated in virions and infected cells (16, 17), and the activation of the DNA damage response (DDR) promotes the recruitment of DNA repair factors to viral genomes through epigenetic modifications of the viral chromatin (18–21). In response to DSBs, ATM phosphorylates the histone H2AX at serine 139, which is referred to as γH2AX (22). γH2AX then coordinates the recruitment of DDR effectors to the damaged sites to facilitate DNA repair. Several DDR-associated epigenetic regulators have been implicated in HPV replication (20). γH2AX is bound to HPV chromatin and colocalizes with HPV replication compartments (23). The E3 ubiquitin ligase RNF168 ubiquitinates the histones H2A/H2AX on lysine 13/15 to promote 53BP1 and BRCA1 recruitment to DSBs, and we have shown that RNF168 is required for productive viral replication (24, 25). In addition, the Tip60 acetyltransferase and SIRT1 deacetylase promote the recruitment of homologous recombination factors to HPV genomes via modifications of viral chromatin (21, 26–29). These studies demonstrate that HPV chromatin modifications are accompanied by the recruitment of DDR effectors that are essential for productive viral replication.

We previously showed that the histone methyltransferase SETD2 plays a key role in promoting the productive replication of HPV31 upon differentiation (30). SETD2 interacts with the phosphorylated C-terminal domain of RNA polymerase II (RNAPII) during transcription elongation and catalyzes the trimethylation of histone H3K36 (H3K36me3) (31–33). By promoting the recruitment of H3K36me3 readers, SETD2 regulates several cellular processes that are also important for the HPV life cycle, including DNA repair and alternative splicing (30, 34–36). We previously found that the HPV31 genome is enriched for H3K36me3 in a

SETD2-dependent manner (30). Additionally, we found that ATM kinase activity is necessary for H3K36me3 maintenance on viral chromatin (30). While these findings indicate that HPV requires SETD2-mediated H3K36me3 for productive viral replication, the manner in which SETD2 and H3K36me3 contribute to viral replication is unclear.

Recent studies have shown that SETD2 promotes HR repair of DSBs in active genes through the constitutive binding of LEDGF to H3K36me3 through its PWWP domain (34). Our previous studies showed that the Rad51 recombinase, which is critical to HR repair, is bound to HPV chromatin and is required for productive replication (37). However, whether SETD2 and H3K36me3 contribute to Rad51 recruitment is currently unclear. In response to DNA damage, LEDGF recruits the C-terminal binding protein interacting protein (CtIP), which promotes DSB end resection with Mre11 of the MRN complex (Mre11, Rad50, Nbs1) (38, 39). End resection is necessary to initiate HR and results in the formation of ssDNA that is bound by replication protein A (RPA), which is subsequently replaced by Rad51 (40). SETD2 also promotes HR factor recruitment in response to replication stress via the constitutive binding of PALB2 to the H3K36me3 effector MRG15 (41). PALB2 serves to physically link BRCA1 and BRCA2 at sites of DNA damage to rapidly recruit Rad51 and to stabilize and/or repair stalled replication forks (42).

Previous studies from our lab suggest that resection occurs on viral DNA during productive replication, including the localization of the resection marker RPA to viral replication foci as well as the requirement for Mre11 nuclease activity in viral genome amplification upon differentiation (15, 37, 43). In this study, we examined whether SETD2 and H3K36me3 contribute to productive replication via Rad51 recruitment through the LEDGF-CtIP axis. We found that SETD2 depletion results in a significant increase of γH2AX on viral chromatin upon differentiation, suggesting that SETD2 is important in promoting repair of viral DNA. In support of this, we found that SETD2 depletion impacts the recruitment of Rad51 to viral DNA. We also found that the inhibition of transcription results in an accumulation of γH2AX on viral DNA and a reduction in Rad51 binding, indicating that transcription promotes viral genomic integrity. Furthermore, we show that SETD2-mediated H3K36me3 recruits LEDGF and CtIP to viral DNA upon differentiation and that CtIP depletion results in a loss of Rad51 binding to viral DNA. We also demonstrate that LEDGF and CtIP are required for productive replication. Together, these results indicate that the enrichment of SETD2-mediated H3K36me3 on transcriptionally active viral genes promotes the rapid repair of viral DNA through the LEDGF-CtIP-Rad51 axis.

RESULTS

SETD2 depletion and H3K36me3 deficiency result in γH2AX accumulation on HPV DNA upon differentiation. Our previous studies showed that SETD2-mediated H3K36me3 is required for productive viral replication (30). H3K36me3-enriched sites are less prone to chromosomal breakage, and reduced H3K36me3 is associated with increased replication stress and DNA damage (44). To determine whether SETD2 facilitates the repair of HPV DNA, we first examined the effect of SETD2 depletion on the accumulation of γH2AX, which is a marker of DNA double-stranded breaks (DSBs), on viral DNA via chromatin immunoprecipitation (ChIP), coupled with qPCR, using primers to different regions of the HPV31 genome, as previously described (30). For these studies, we used the CIN612 cell line, which is derived from a CIN1 cervical lesion and stably maintains HPV31 genomes. We previously used CIN612 cells to define the role of SETD2 and H3K36me3 in the HPV31 life cycle (30). As we showed previously, γH2AX is detected on HPV31 DNA in undifferentiated cells, and the levels of γH2AX increase significantly upon differentiation in high-calcium medium, which has been shown to activate the productive phase of the life cycle by 48 h post-exposure (Fig. 1A) (23). We found that the depletion of SETD2 using our validated shRNAs resulted in a decrease in γH2AX on the viral chromatin in undifferentiated cells (Fig. 1B and D) (30). In contrast, a significant increase in γH2AX accumulation was observed on viral DNA upon differentiation, suggesting that SETD2 is important in the maintenance of viral DNA integrity during the productive phase of the viral life cycle (Fig. 1E). We observed a moderate increase in the global levels of γH2AX in differentiating cells upon the depletion of SETD2 (Fig. 1F), which is consistent with the finding of

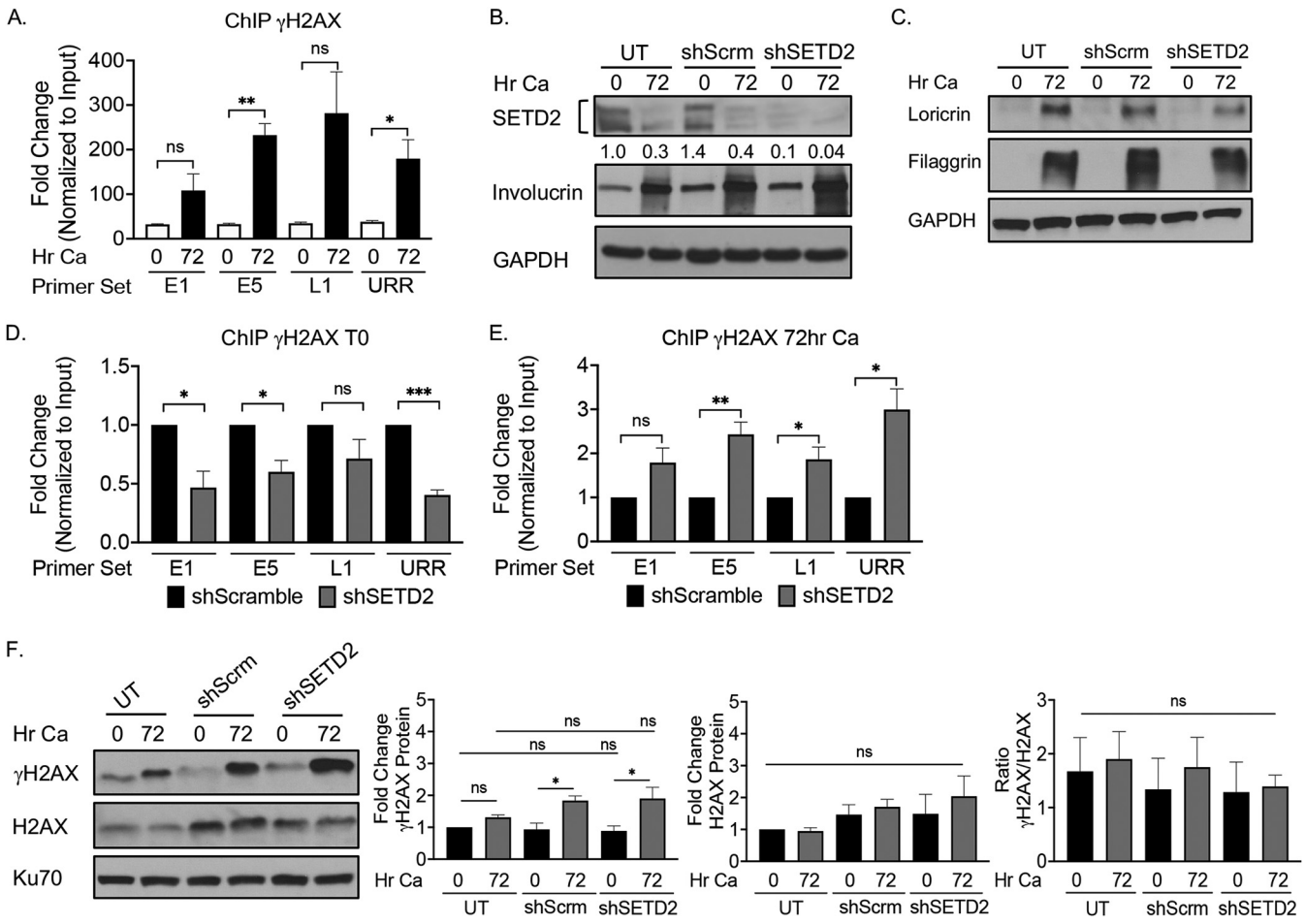

FIG 1 SETD2 depletion leads to increased γH2AX accumulation on HPV DNA. (A) Chromatin was harvested from CIN612 cells that were undifferentiated (0 h) or differentiated in high-calcium medium for 72 h. ChIP was performed using an antibody to IgG or γH2AX, and this was followed by quantitative PCR (qPCR) using primer pairs to the HPV31 E1 and E5 as well as the L1 open reading frame or the untranslated regulatory region (URR). Data from three independent experiments are represented as the fold enrichment over the IgG control for each time point. The values for each time point were normalized to the input values that were amplified in parallel to control for changes in the episome copy number upon differentiation. (B–F) CIN612 cells were left untreated or transiently transduced with a scramble control shRNA (shScrm) or shRNA that was specific to SETD2 (shSETD2) for 72 h. Cells were harvested as an undifferentiated sample (T0) or induced to differentiate in high calcium medium for 72 h. Protein and chromatin were harvested at each time point. (B) A Western blot analysis was performed using antibodies to SETD2, involucrin as a differentiation control, and GAPDH as a loading control. The densitometry for SETD2 depletion was carried out using ImageJ. The protein levels were normalized to GAPDH, with the undifferentiated untreated sample (UT T0) being set to one. (C) A Western blot analysis was performed on urea-solubilized proteins using antibodies to loricrin, filaggrin, and GAPH as a loading control. (D and E) γH2AX ChIP coupled with qPCR was carried out, using the indicated primer pairs to the HPV31 genome. To control for the increase in the viral copy number upon differentiation, PCR data from three independent experiments were normalized to the input values that were quantified in parallel. Values are expressed as the fold changes in γH2AX binding, relative to the shScramble control, which is set to one for each primer pair. (F) A Western blot analysis was performed using antibodies to γH2AX, total H2AX, and Ku70 as a loading control. The densitometry for γH2AX and H2AX was performed across three independent experiments using ImageJ. The protein levels were normalized to Ku70. The values are expressed as fold changes, relative to UT T0, which is set to one. (B, C, and F) Representative images of three independent experiments are shown. Statistical significance was determined using a Student's *t* test. Error bars represent the mean ± the standard error. *, $P \leq 0.05$; **, $P \leq 0.01$; ***, $P \leq 0.001$; ns, not significant. Ca, calcium.

previous reports that identified a role for SETD2 in the maintenance of cellular genomic integrity (34). Importantly, epithelial differentiation was not impacted by SETD2 depletion, as was demonstrated by the increase in the early differentiation marker involucrin and the terminal differentiation markers loricrin and filaggrin (Fig. 1B and C).

To determine whether H3K36me3 plays a role in maintaining viral genome integrity, we transiently overexpressed an H3.3 lysine 36 to methionine mutant that cannot be methylated (H3.3K36M) and also reduces the levels of H3K36me3 on endogenous histones by targeting the active site of SETD2, thereby competing for substrate binding and turnover (45). In alignment with the results of our previous study (30), H3.3K36M expression resulted in a global decrease in H3K36me3 levels without affecting epithelial differentiation, as evidenced by the increase in involucrin (Fig. 2A). In contrast to the

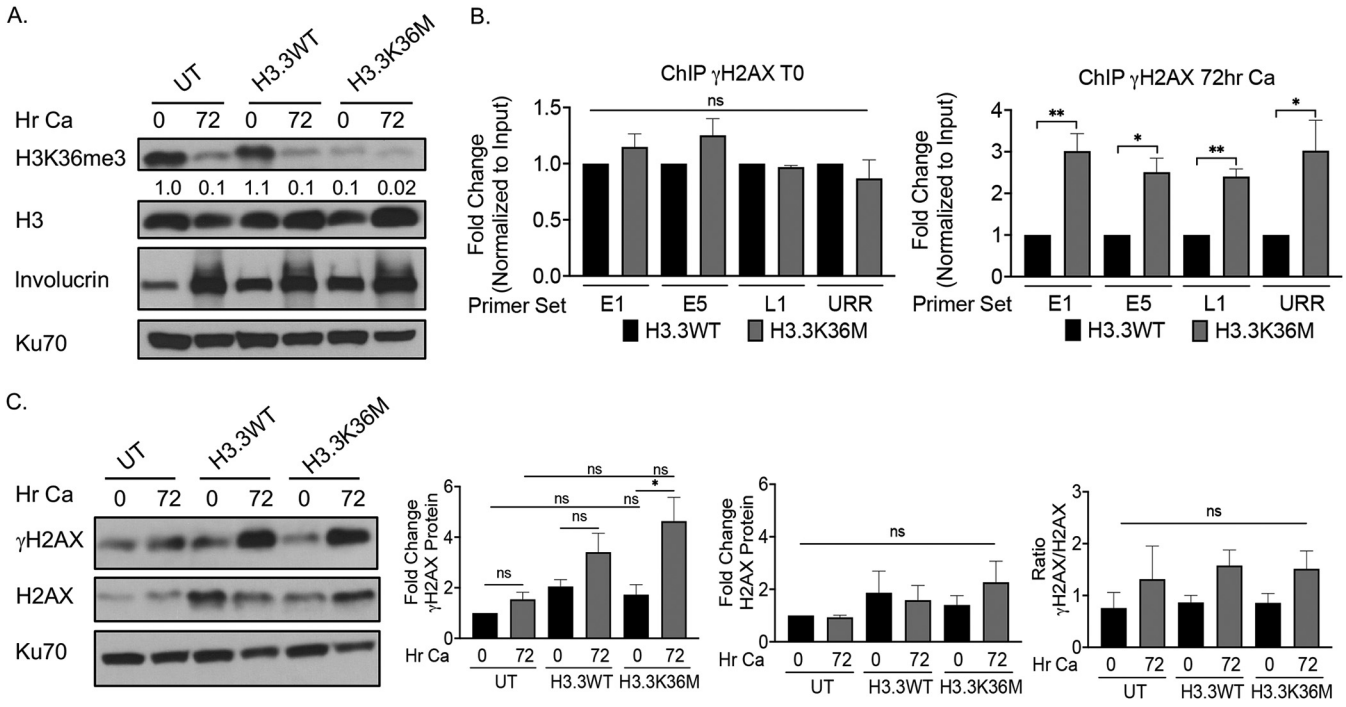

FIG 2 The depletion of H3K36me3 results in increased γH2AX accumulation on HPV chromatin. (A–C) CIN612 cells were left untreated or transiently transduced with either wild-type H3.3 (H3.3WT) or the H3.3K36M mutant for 72 h. Cells were harvested as an undifferentiated sample (T0) or induced to differentiate in high calcium medium for 72 h. Protein and chromatin were harvested at each time point. (A) A Western blot analysis was performed using antibodies to H3K36me3, histone H3, involucrin as a differentiation control, and Ku70 as a loading control. The densitometry for H3K36me3 was performed using ImageJ. The protein levels were normalized to H3, with the T0 untreated (UT) sample set to one. (B) ChIP was performed for γH2AX coupled with qPCR, using the indicated primer pairs to the HPV31 genome. The ChIP data from three independent experiments were normalized to the input values that were quantified in parallel. The values are expressed as fold changes in γH2AX binding, relative to the H3.3WT control, which is set to one for each primer pair. (C) A Western blot analysis was performed using antibodies to γH2AX, total H2AX, and Ku70 as a loading control. The densitometry for γH2AX and H2AX was performed across three independent experiments using ImageJ. The protein levels were normalized to Ku70. The values are expressed as fold changes, relative to UT T0, which is set to one. (A and C) Representative images of three independent experiments are shown. Statistical significance was determined using a Student's *t* test. Error bars represent the mean ± the standard error. *, $P \leq 0.05$; **, $P \leq 0.01$; ns, not significant. Ca, calcium.

depletion of SETD2, the overexpression of H3.3K36M minimally affected the levels of γH2AX on viral DNA in undifferentiated cells (Fig. 2B). However, upon differentiation, H3K36me3 deficiency resulted in a further accumulation of γH2AX on viral DNA, similar to that observed upon SETD2 depletion (Fig. 2B). The global levels of γH2AX were modestly altered by H3.3K36M overexpression, compared to H3.3 overexpression (Fig. 2C). These results indicate that H3K36me3 on viral chromatin is important for promoting the repair of damaged viral DNA upon differentiation. Intriguingly, the finding that γH2AX decreases on viral DNA upon SETD2 depletion but not upon H3.3K36M overexpression suggests that SETD2 may facilitate upstream signaling events in DDR activation independently of H3K36me3 during episomal maintenance.

Transcriptionally active loci are prone to chromosomal breakage and exhibit a preference for HR repair that is regulated by the SETD2-mediated placement of H3K36me3 during transcription elongation (46, 47). We previously showed that H3K36me3 enrichment on HPV31 chromatin occurs in a SETD2-dependent manner (30). To determine whether transcription contributes to viral genome integrity, we transiently inhibited transcription using α-amanitin, which promotes RNA pol II degradation, as previously described (41). As shown in Fig. 3A, 17 h of treatment with α-amanitin resulted in a reduction in 5-ethynyluridine (EU) incorporation in undifferentiated and differentiated CIN612 cells, indicating the successful inhibition of transcription. Similar to SETD2 depletion and H3.3K36M expression, we found that transcription inhibition also resulted in an increase in γH2AX accumulation on viral chromatin upon differentiation, and this occurred without a marked effect on global γH2AX levels (Fig. 3B–D). These results indicate that active transcription protects viral DNA from damage, possibly via the placement of H3K36me3 by SETD2.

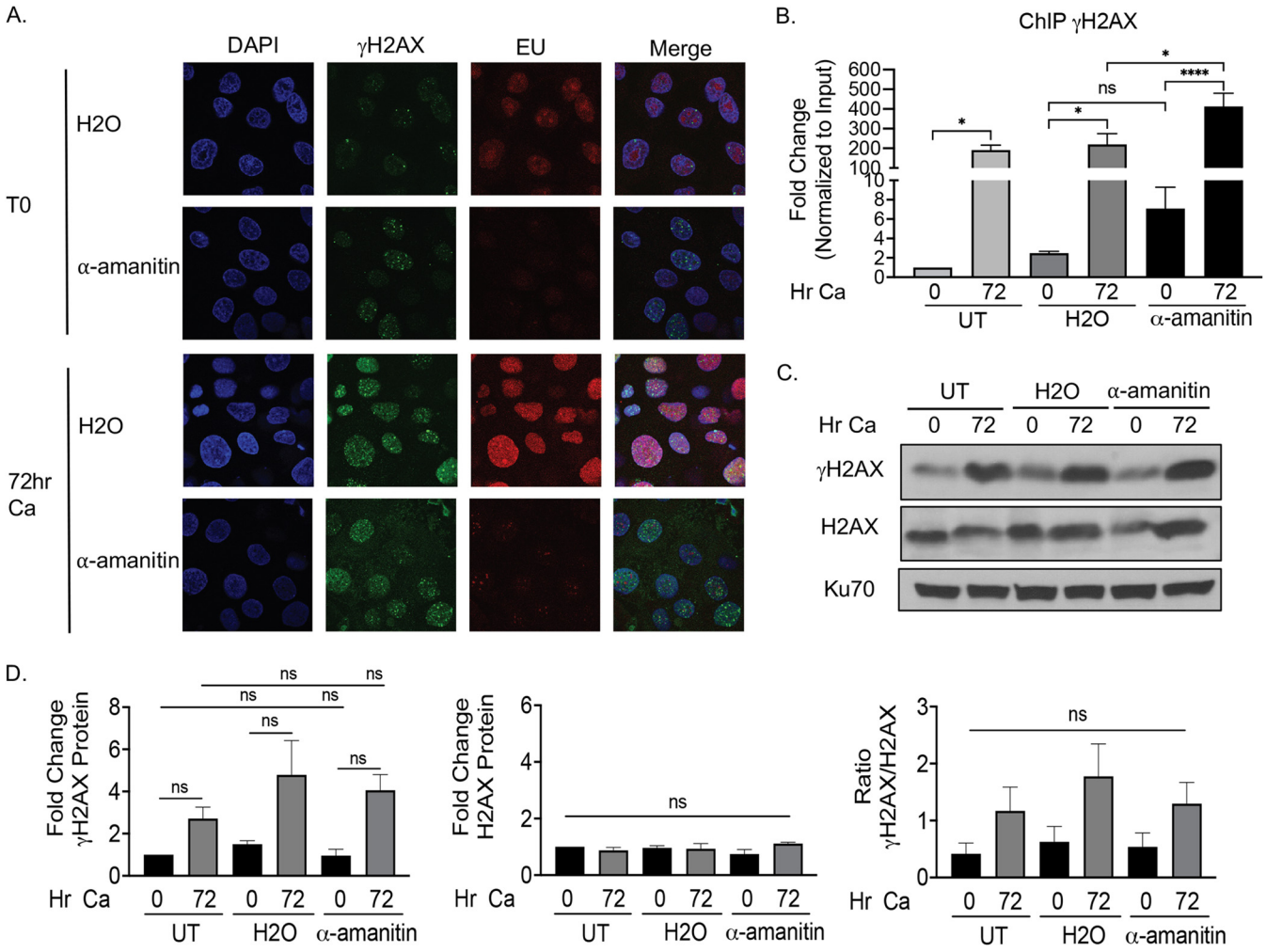

FIG 3 The inhibition of transcription increases γH2AX accumulation on HPV chromatin. (A) Immunostaining was performed on undifferentiated (T0) or differentiated (72 h Ca) CIN612 cells that were left untreated (UT), treated with vehicle control (H2O), or treated with α-amanitin (4 μg/mL) for 17 h before harvest. EU was added 1 h prior to harvest and developed using the Click-iT RNA protocol. Representative images of γH2AX, EU, and DAPI staining are shown from three independent experiments. Images were collected on a Zeiss 710 confocal laser-scanning microscope. (B) ChIP-qPCR for γH2AX was performed on chromatin that was harvested from the samples described in panel A, using primers to the E5 open reading frame. To control for changes in the viral copy number upon differentiation, ChIP data from three independent experiments were normalized to the input values that were quantified in parallel. Values are expressed as fold changes in γH2AX binding, relative to the UT T0 sample, which was set to 1. (C) A Western blot was performed using antibodies to γH2AX, total H2AX, and Ku70 as a loading control. A representative image from three independent experiments is shown. (D) The densitometry for γH2AX and H2AX was performed across three independent experiments using ImageJ. The protein levels were normalized to Ku70 and expressed as fold changes, relative to the UT T0, which was set to 1. Statistical significance was determined using a one-way analysis of variance (ANOVA). The error bars represent ± the standard error of the mean. *, $P \leq 0.05$; ****, $P \leq 0.0001$; ns, not significant. Ca, calcium.

Rad51 is recruited to viral DNA in a SETD2-dependent and H3K36me3-dependent manner. SETD2-mediated H3K36me3 promotes the HR repair of DSBs in actively transcribed genes via the recruitment of Rad51 (34, 41). To determine whether the increase in γH2AX accumulation on viral DNA upon SETD2 depletion corresponded with a decrease in Rad51 recruitment, we performed ChIP, coupled with qPCR, using several primer pairs across the HPV31 genome. As we showed previously (37), Rad51 binding to viral DNA increases upon differentiation (Fig. 4A). Interestingly, SETD2 depletion resulted in a significant decrease in Rad51 recruitment to viral DNA in both undifferentiated and differentiated cells (Fig. 4B and C), with moderate changes in the Rad51 protein levels only occurring upon differentiation (Fig. 4D). H3.3K36M overexpression also resulted in impaired Rad51 binding to viral DNA in both undifferentiated and differentiated cells, compared to WT H3.3 (Fig. 4E and F), with minimal effect on global Rad51 levels (Fig. 4G). Furthermore, we found that the transient treatment of CIN612 cells with α-amanitin also resulted in a decrease in Rad51 recruitment to HPV DNA, but this occurred only upon differentiation

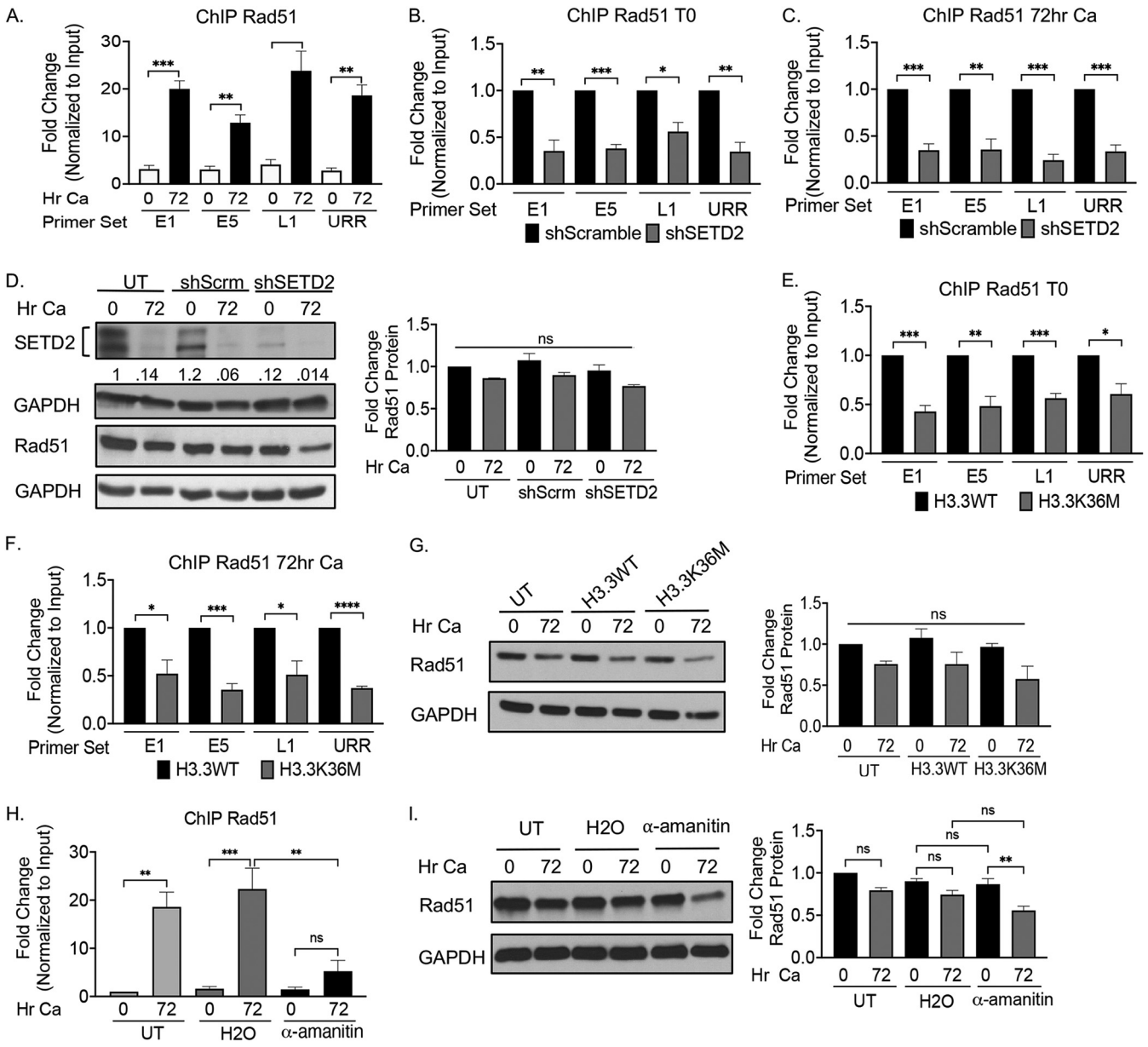

FIG 4 SETD2 and H3K36me3 promote Rad51 recruitment to HPV DNA. (A) Chromatin was harvested from CIN612 cells that were either undifferentiated (T0) or differentiated in high-calcium medium for 72 h. ChIP was performed using an antibody to IgG or Rad51, and this was followed by qPCR, using primer pairs to the indicated regions of the HPV31 genome. Data from three independent experiments are represented as the fold enrichment over the IgG control for each time point. The values for each time point were normalized to the input values that were amplified in parallel to control for changes in the episome copy number upon differentiation. (B–G) CIN612 cells were left untreated or transiently transduced with a scramble control shRNA (shScrm), shRNA specific to SETD2 (shSETD2), wild-type H3.3 (H3.3WT), or the H3.3K36M mutant for 72 h. The cells were harvested as an undifferentiated sample (T0) or induced to differentiate in high calcium medium for 72 h. Protein and chromatin were harvested at the indicated time points (B, C). ChIP was performed for Rad51 coupled with qPCR, using the indicated primers to the HPV31 genome. To control for the viral copy number, ChIP data from three independent experiments were normalized the input values that were quantified in parallel. The values are expressed as fold changes in Rad51 binding, relative to the shScramble control, which was set to 1 for each primer pair. (D) A Western blot analysis was performed using antibodies to SETD2 and Rad51, with GAPDH as a loading control. The densitometry for the SETD2 protein levels was carried out using ImageJ. The protein levels were normalized to GAPDH, with UT T0 being set to 1. (E, F) ChIP was performed for Rad51 coupled with qPCR, using the indicated primer pairs to the HPV31 genome. To control for the viral copy number, ChIP data from three independent experiments were normalized to the input values that were quantified in parallel. The values are expressed as the fold change in Rad51 binding, relative to the H3.3WT control, which was set to 1 for each primer pair. (G) A Western blot analysis was performed using antibodies to Rad51, with GAPDH as a loading control. The densitometry for Rad51 was performed across three independent experiments using ImageJ. The protein levels were normalized to GAPDH, and the values were expressed as the fold change, relative to UT T0, which was set to 1. (H, I) Undifferentiated (T0) or differentiated (72 h Ca) CIN612 cells were left untreated (UT) or were treated with vehicle control (H2O) or α-amanitin (4 μg/mL) for 17 h before harvest. Protein and chromatin were harvested at each time point. (H) ChIP-qPCR for Rad51 was performed using primers to the E5 open reading frame. ChIP data from three independent experiments were normalized to the input values that were quantified in parallel to control for the viral copy number. The values were expressed as the fold change in Rad51 binding, relative to the UT T0 sample, which was set to 1. (I) A Western blot analysis was performed on lysates that were harvested from the indicated samples using antibodies to Rad51, with GAPDH as a loading control. The densitometry

(Continued on next page)

and with a modest effect on Rad51 protein levels, compared to the H_2O control (Fig. 4H and I). Overall, these results suggest that the SETD2-mediated trimethylation of H3K36 during viral transcription upon differentiation promotes the repair of damaged viral DNA through the recruitment of Rad51.

LEDGF recruitment to HPV chromatin requires SETD2 and H3K36me3. SETD2-mediated H3K36me3 protects actively transcribed genes from replication stress and promotes DSB repair through the MRG15/PALB2 pathway as well as the LEDGF/CtIP pathway, respectively (34, 39, 41). Since our previous studies suggest that DSB resection occurs on viral DNA (12, 43), we examined whether SETD2 recruits Rad51 through the LEDGF/CtIP pathway. LEDGF levels were previously shown to be elevated in multiple HPV-positive cancer cell lines containing integrated viral genomes (48). In undifferentiated cells, we found the LEDGF protein and mRNA levels to be similar between undifferentiated control human foreskin keratinocytes (HFKs) and CIN612 cells (Fig. 5A and B). However, upon differentiation, the LEDGF protein levels rapidly declined in the HFKs but were maintained in the CIN612 cells, along with increased LEDGF mRNA (Fig. 5A and B). Similar results were observed in HFKs stably maintaining HPV-31 genomes (HFK-31), compared to matched uninfected HFKs (Fig. 5C and D). Using ChIP, coupled with qPCR, we detected a moderate increase in LEDGF binding to viral DNA in undifferentiated cells (T0), compared to the IgG control (Fig. 5E). However, LEDGF binding significantly increased upon differentiation across the viral genome, suggesting that LEDGF plays a more prominent role during late viral events. Consistent with the low levels of LEDGF bound to viral DNA in undifferentiated cells, SETD2 depletion led to a minimal reduction in LEDGF binding to viral DNA, compared to that observed with control cells (Fig. 5F). However, upon differentiation, a significant decrease in LEDGF binding occurred, and this occurrence had no discernible effect on the global LEDGF levels (Fig. 5G and H). A similar phenotype was observed upon the expression of H3.3K36M, compared to WT H3.3 (Fig. 5I–K). Overall, these results indicate that LEDGF is recruited to viral DNA upon differentiation in a SETD2-dependent and H3K36me3-dependent manner.

CtIP recruitment to viral DNA requires SETD2 and H3K36me3. The constitutive binding of LEDGF to H3K36me3 serves as a docking site for CtIP in response to DNA damage (34, 39). CtIP interacts with the MRN complex to initiate end resection with the Mre11 and also interacts with BRCA1 to increase resection efficiency (49). End resection is critical in the blocking of error-prone nonhomologous end joining repair and in the initiation of HR (40). Based on our observation that SETD2 and H3K36me3 promote LEDGF and Rad51 recruitment to viral DNA, we next wanted to determine whether CtIP is also recruited to viral DNA. We found that CtIP protein levels are increased in undifferentiated CIN612 cells as well as HFK-31 cells, compared to uninfected HFKs (Fig. 6A and B). However, CtIP levels dramatically decreased upon differentiation in HFKs as well as in CIN612 and HFK-31 cells, despite an increase in CtIP mRNA (Fig. 6A–D). Using ChIP, coupled with qPCR, we detected minimal CtIP binding to viral DNA in undifferentiated cells (Fig. 6E). However, CtIP recruitment to viral DNA significantly increased upon differentiation, despite the drastic reduction in CtIP protein levels (Fig. 6E). Given that CtIP is a DNA damage response protein (49), these results further suggest that viral genome amplification and/or late gene expression renders viral DNA susceptible to DNA damage. Not surprisingly, we found that SETD2 depletion did not affect CtIP binding to viral DNA in undifferentiated cells but did result in a significant decrease in CtIP binding upon differentiation (Fig. 6F). The overexpression of the H3.3K36M mutant yielded a similar phenotype, with reduced CtIP binding being observed upon differentiation (Fig. 6H). Neither SETD2 depletion nor H3.3K36M expression affected the global CtIP levels (Fig. 6G and I), indicating that the loss of CtIP

FIG 4 Legend (Continued)

for Rad51 was performed across three independent experiments using ImageJ. The protein levels were normalized to the GAPDH loading control, and the values were expressed as the fold change, relative to UT T0, which was set to 1. (D, G, I) Representative images from three independent experiments are shown. Statistical significance was determined using a Student's *t* test. The error bars represent the mean ± the standard error. *, $P \leq 0.05$; **, $P \leq 0.01$; ***, $P \leq 0.001$; ****, $P \leq 0.0001$; ns, not significant. Ca, calcium.

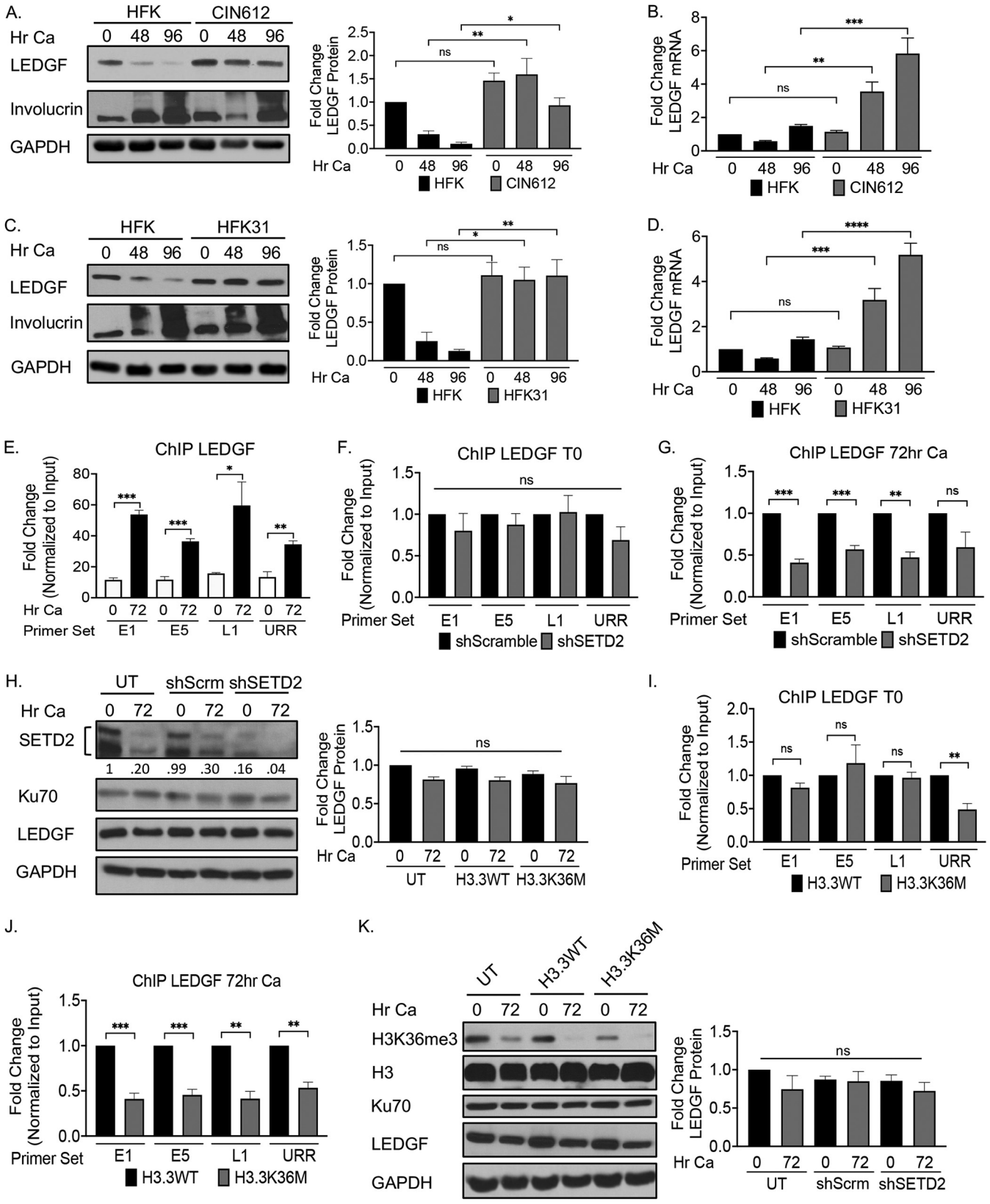

FIG 5 LEDGF is recruited to HPV chromatin in a SETD2-dependent and H3K36me3-dependent manner. (A–D) Human foreskin keratinocytes (HFKs), CIN612, and HFK-31 cells were harvested as an undifferentiated sample (T0) or induced to differentiate in high calcium medium for 48 and 96 h. (A, C) A Western blot analysis was performed using antibodies to LEDGF, involucrin as a differentiation control, and GAPDH as a loading control. The densitometry for LEDGF was performed across three independent experiments using ImageJ. The protein levels were normalized to GAPDH, and the values are expressed as

(Continued on next page)

binding to viral chromatin is due to a decrease in H3K36me3 and not reduced levels of CtIP. Furthermore, SETD2 depletion did not affect the recruitment of Nbs1 of the MRN complex to viral DNA (Fig. 6J), which can also recruit CtIP to DSBs to initiate DNA end resection (40). Overall, these results, coupled with our finding that LEDGF binds to viral DNA in a H3K36me3-dependent manner, suggest that CtIP is recruited to damaged viral DNA upon differentiation via the H3K36me3-LEDGF pathway.

CtIP is required for Rad51 recruitment to viral DNA upon differentiation. To determine whether CtIP influences the repair of viral DNA, we performed ChIP for γH2AX and Rad51 on chromatin that was harvested from undifferentiated and differentiated CIN612 cells that were transiently transduced with either the control shRNA (shScramble) or validated shRNAs specific for CtIP (Fig. 7) (50). Whereas CtIP knockdown had no discernible effect on the γH2AX levels on viral DNA in undifferentiated cells, a significant increase in γH2AX accumulation on viral DNA occurred upon differentiation, and this was accompanied by a significant decrease in Rad51 binding (Fig. 7A and C). Importantly, the global levels of γH2AX and Rad51 were not affected by CtIP depletion (Fig. 7B and D). To ensure that the reduction in Rad51 recruitment was not due to the removal of LEDGF from viral chromatin, we examined LEDGF binding to viral DNA upon CtIP depletion. Importantly, we found that CtIP knockdown did not affect LEDGF binding to viral DNA in undifferentiated or differentiated cells (Fig. 7E). Overall, these data suggest that CtIP is recruited to viral DNA upon differentiation via the SETD2-H3K36me3-LEDGF pathway, thereby promoting end resection that recruits Rad51 to facilitate repair.

LEDGF and CtIP are required for productive replication. The increase in binding of LEDGF and CtIP to HPV chromatin upon differentiation, coupled with the requirement of CtIP in Rad51 recruitment to viral DNA, indicates that these factors are important in viral genome amplification. To examine this, we transiently knocked down LEDGF and CtIP using our validated shRNAs (50, 51) (Fig. 8A). While LEDGF depletion moderately affected cell growth, we were unable to induce differentiation in a high-calcium medium, which requires the maintenance of a confluent monolayer. Instead, we induced differentiation via suspension in methylcellulose, which triggers the productive phase of the viral life cycle by 24 h post-suspension (52). As shown in Fig. 8, the depletion of LEDGF as well as CtIP had modest effects on episomal maintenance in undifferentiated cells. However, LEDGF-depleted and CtIP-depleted cells failed to efficiently amplify viral genomes upon differentiation (Fig. 8B and C). This finding is consistent with the significant increase in the binding of LEDGF and CtIP to viral DNA upon differentiation. Importantly, LEDGF and CtIP knockdown did not impede differentiation, as shown by the differentiation-specific marker involucrin (Fig. 8A). This indicates that the effect on viral genome amplification is not an indirect effect of inhibiting cellular differentiation. We also confirmed the requirement of CtIP in productive replication using calcium-induced differentiation (Fig. 8D–F). HPVs amplify their genomes

FIG 5 Legend (Continued)
fold changes, relative to the HFK T0, which was set to 1. (B, D) Total RNA was extracted from the indicated samples, and RT-qPCR was performed using primers specific to LEDGF. Fold changes were calculated using the $2^{-\Delta\Delta CT}$ method. The fold change relative to HFK T0, which was set to 1, is shown. (E) Chromatin was harvested from CIN612 cells that were undifferentiated (T0) or differentiated in high-calcium medium for 72 h. ChIP was performed using an antibody to IgG or LEDGF, and this was followed by qPCR, using the indicated primer pairs to the HPV31 genome. ChIP data from three independent experiments is represented as the fold enrichment over the IgG control for each time point. The values for each time point were normalized to the input values that were amplified in parallel to control for changes in the episome copy number upon differentiation. (F–K) CIN612 cells were left untreated or transiently transduced with a scramble control shRNA (shScrm), shRNA specific to SETD2 (shSETD2), wild-type H3.3 (H3.3WT), or the H3.3K36M mutant for 72 h as an undifferentiated sample (T0) or were induced to differentiate in high calcium medium for 72 h. Protein and chromatin were harvested at each time point. (F, G, I, J) ChIP-pPCR for LEDGF was performed using the indicated primer sets to the HPV31 genome. ChIP data from three independent experiments were normalized to input values that were quantified in parallel to control for changes in the viral copy number upon differentiation. The values are expressed as the fold change in LEDGF binding, relative to either the shScramble control (panels F and G) or the H3.3 WT (panels I and J), which were set to 1 for each primer pair. (H) A Western blot analysis was performed using antibodies to SETD2 and LEDGF, with GAPDH and Ku70 as loading controls. The densitometry for the SETD2 depletion was carried out using ImageJ. The protein levels were normalized to Ku70 and expressed as the fold change, relative to the UT T0 sample, which was set to 1. The densitometry for LEDGF was performed across three independent experiments using ImageJ. The protein levels were normalized to GAPDH, with the UT T0 being set to 1. (K) A Western blot analysis was performed using antibodies to H3K36me3, H3, and LEDGF, with Ku70 and GAPDH as loading controls. The densitometry for LEDGF was performed across three independent experiments using ImageJ. The protein levels were normalized to GAPDH, with the values expressed as the fold change, relative to UT T0, which was set to 1. Statistical significance was determined using a Student's *t* test. The error bars represent the mean ± the standard error. *, $P \leq 0.05$; **, $P \leq 0.01$; ***, $P \leq 0.001$; ****, $P \leq 0.0001$; ns, not significant. Ca, calcium.

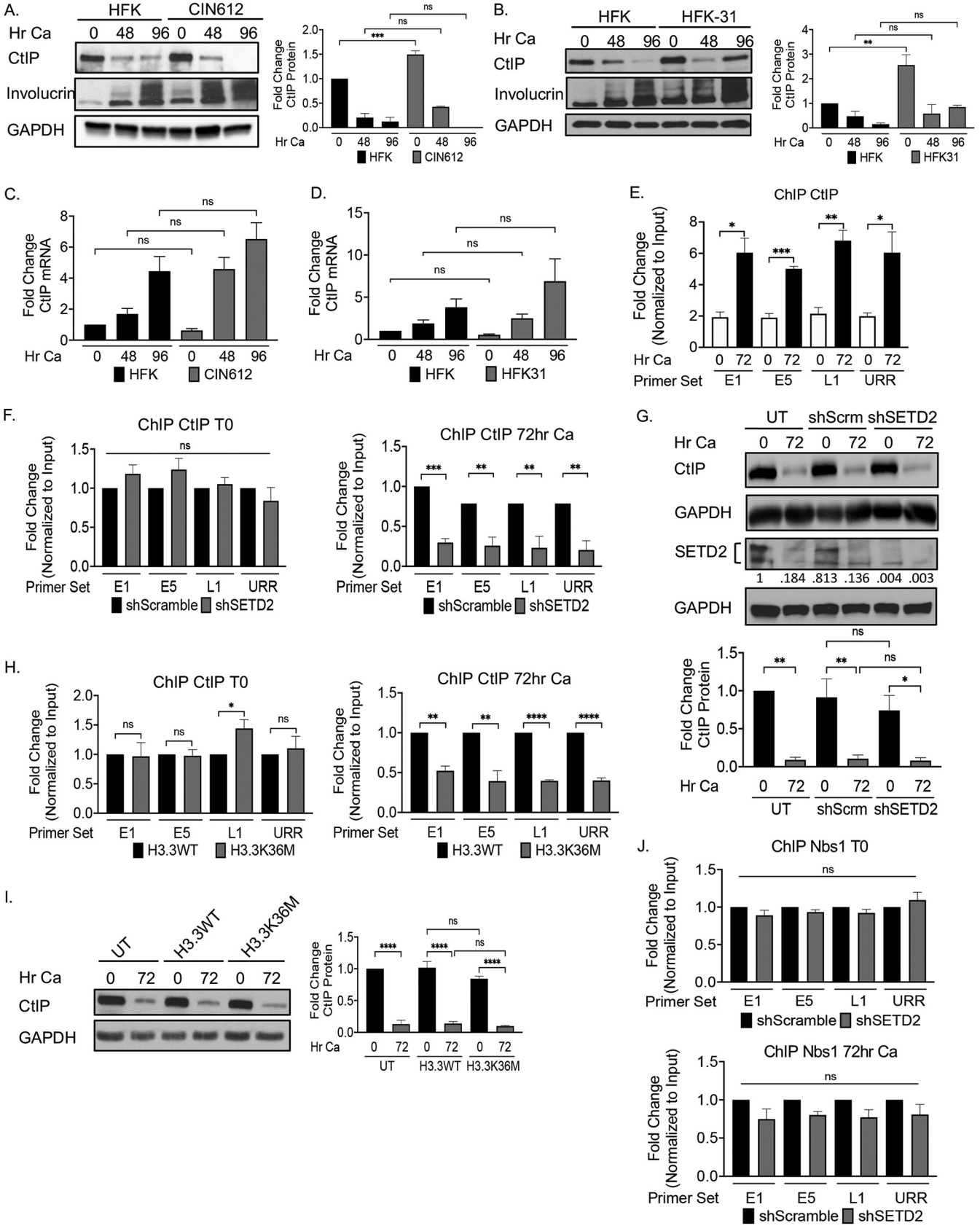

FIG 6 CtIP is recruited to HPV DNA in a SETD2-dependent and H3K36me3-dependent manner. (A–D) Human foreskin keratinocytes (HFKs), CIN612, and HFK-31 cells were harvested as an undifferentiated sample (T0) or induced to differentiate in high calcium medium for 48 or 96 h. (A, B) A Western blot

(Continued on next page)

in a G_2-arrested environment (53). Previous studies showed that LEDGF depletion results in an accumulation of cells in the S and G_2 phases, indicating that the effect observed on viral replication upon knockdown is not due to an indirect effect on the cell cycle (38). Additionally, CtIP depletion has been shown to have little effect on the cell cycle (54). Overall, these results indicate that LEDGF and CtIP play important roles in promoting viral replication in differentiating cells, presumably through the repair of damaged viral DNA via the recruitment of Rad51 (Fig. 9).

DISCUSSION

Previous studies from our lab established a critical role for HR repair factors in supporting viral genome amplification in differentiating cells, including the MRN complex, BRCA1, and Rad51 (23, 37, 43). In this study, we demonstrate that SETD2-mediated H3K36me3 protects the genomic integrity of HPV31 upon differentiation through the recruitment of Rad51. We demonstrate that LEDGF and CtIP bind to viral chromatin in a SETD2-dependent and H3K36me3-dependent manner and are required for productive replication. In addition, we show that CtIP mediates the recruitment of Rad51 to viral DNA upon differentiation to support productive viral replication. Overall, our data identify a novel role for SETD2-mediated H3K36me3 in the epigenetic regulation of the viral life cycle by supporting the HR repair of viral DNA through the LEDGF-CtIP axis.

γH2AX accumulates on viral DNA upon differentiation, indicating that late viral events result in DNA damage that must be repaired for the successful completion of the viral life cycle. A critical role has been established for the ATM DNA damage response pathway in the facilitation of viral genome amplification through epigenetic modifications of viral chromatin, including the maintenance of H3K36me3 on viral chromatin (11, 30). In this study, we have found that SETD2 depletion as well as H3.3K36M overexpression result in the further accumulation of γH2AX on viral DNA upon differentiation, and this is accompanied by reduced Rad51 loading, which is suggestive of an increase in DNA damage due to a failure to mediate HR repair. In contrast, in undifferentiated cells SETD2 depletion resulted in reduced γH2AX and Rad51 on viral DNA, suggesting a potential deficiency in DDR initiation on viral chromatin. These contrasting findings indicate that different mechanisms of DDR regulation are employed during episomal maintenance in undifferentiated cells and productive replication upon epithelial differentiation. Additionally, we found that H3.3K36M overexpression in undifferentiated cells reduced Rad51 loading on viral DNA but had no effect on γH2AX accumulation, in contrast to that which was observed with SETD2 depletion. These results suggest that SETD2 may be acting through two different pathways to initiate DDR signaling (H3K36me3-independent) and promote Rad51 recruitment (H3K36me3-dependent) to viral DNA in undifferentiated cells. SETD2 has been

FIG 6 Legend (Continued)
analysis was performed using antibodies to CtIP, involucrin as a differentiation control, and GAPDH as a loading control. The densitometry for CtIP was performed across three independent experiments using ImageJ. The protein levels were normalized to GAPDH, and the values are expressed as the fold change, relative to HFK cells at T0, which was set to 1. (C, D) Total RNA was extracted, and RT-qPCR was performed, using primers specific to CtIP. The fold change was calculated using the $2^{-\Delta\Delta CT}$ method. The fold change, relative to HFK T0, which was set to 1, is shown. (E) Chromatin was harvested from CIN612 cells that were undifferentiated (0 h) or differentiated in high-calcium medium for 72 h. ChIP was performed using an antibody to IgG or CtIP, and this was followed by qPCR, using the indicated primer pairs to the HPV31 genome. Data from three independent experiments are represented as the fold enrichment over the IgG control for each time point. The values for each time point were normalized to the input values that were amplified in parallel to control for changes in the episome copy number upon differentiation. (F–I) CIN612 cells were left untreated or transiently transduced with a scramble control shRNA (shScrm), shRNA specific to SETD2 (shSETD2), H3.3, or H3K36M for 72 h. Cells were harvested as an undifferentiated sample (T0) or induced to differentiate in high calcium medium for 72 h. Protein and chromatin were harvested at each time point. (F, H) ChIP-qPCR was performed for CtIP, using the indicated primer sets. To control for the viral copy number, ChIP data from three independent experiments were normalized to the input values that were quantified in parallel. Values are expressed as the fold change in CtIP binding, relative to the shScramble control or H3.3WT, which were set to 1 for each primer pair. (G) A Western blot analysis was performed using antibodies to CtIP and SETD2, with GAPDH as a loading control. The densitometry for SETD2 protein levels was carried out using ImageJ. The protein levels were normalized to GAPDH and expressed as the fold change, relative to the UT T0 sample, which was set to 1. The densitometry for CtIP was performed across three independent experiments using ImageJ. The protein levels were normalized to GAPDH and are expressed as the fold change, relative to UT T0, which was set to 1. (I) Western blotting was performed using antibodies to CtIP, with GAPDH as a loading control. The densitometry for CtIP was performed across three experiments, as described above. (J) ChIP-qPCR for Nbs1 was performed using the indicated primers to the HPV31 genome. ChIP data from three independent experiments were normalized to input values that were quantified in parallel. Values are expressed as the fold change in Nbs1 binding, relative to the shScramble control, which was set to 1 for each primer pair. Statistical significance was determined using a Student's *t* test. Error bars represent the mean ± the standard error. *, $P \leq 0.05$; **, $P \leq 0.01$; ***, $P \leq 0.001$; ****, $P \leq 0.0001$; ns, not significant. Ca, calcium.

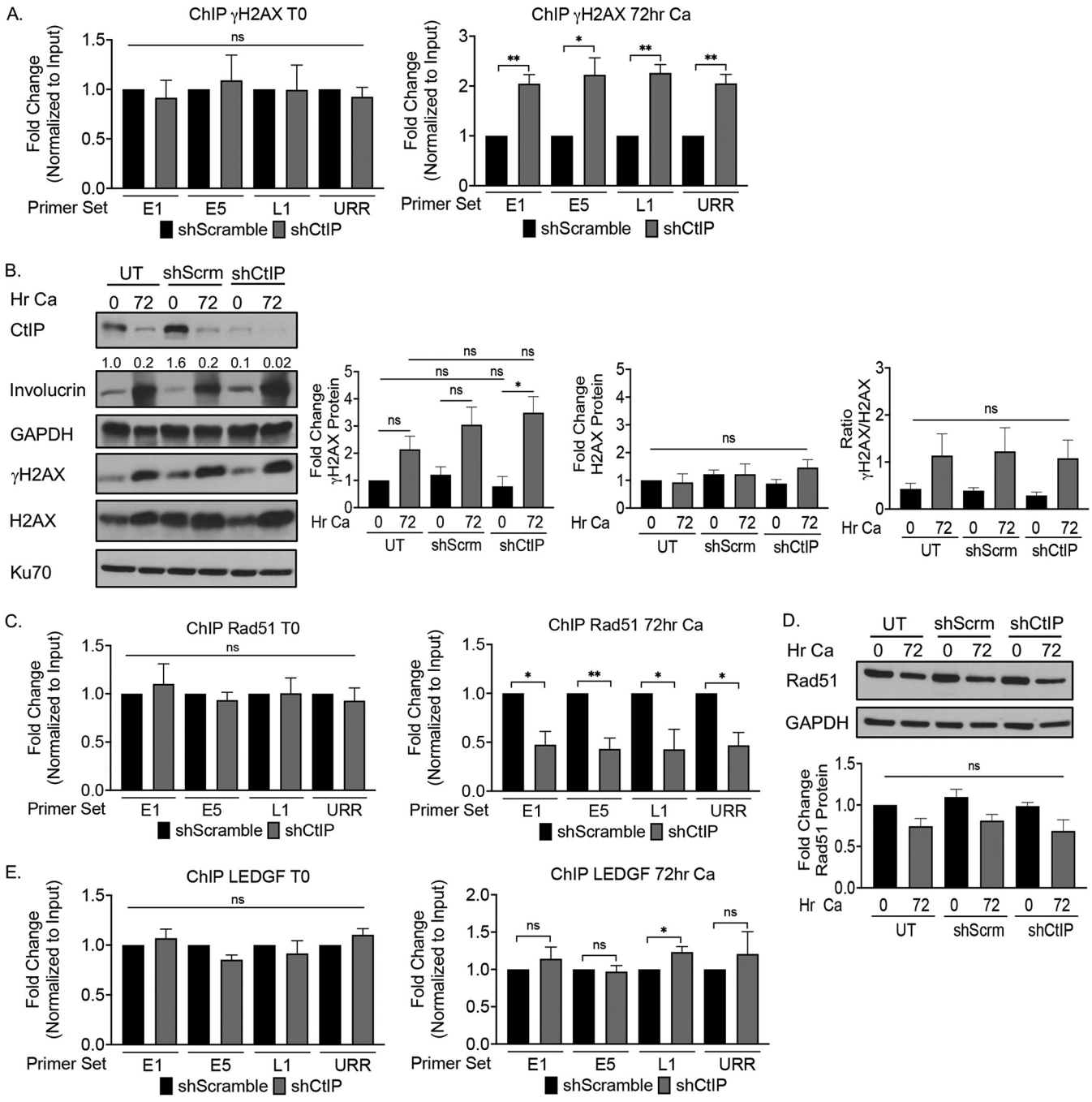

FIG 7 CtIP is required for Rad51 recruitment to viral DNA upon differentiation. (A–E) CIN612 cells were left untreated or transiently transduced with a scramble control shRNA (shScrm) or shRNA specific to CtIP (shCtIP) for 72 h. Cells were harvested as an undifferentiated sample (T0) or induced to differentiate in high calcium medium for 72 h. Protein and chromatin were harvested at each time point. (A, C, E) ChIP-qPCR was performed for γH2AX (panel A), Rad51 (panel C), or LEDGF (panel E), using the indicated primer pairs to the HPV31 genome. To control for the viral genome copy number, ChIP data from three independent experiments were normalized to input values that were quantified in parallel. Values are expressed as the fold change in γH2AX, Rad51, or LEDGF binding, relative to the shScramble control, which was set to 1 for each primer pair. (B) A Western blot analysis was performed using antibodies to CtIP, γH2AX, H2AX, involucrin as differentiation control, and GAPDH and Ku70 as loading controls. The CtIP knockdown efficiency was determined via densitometry using ImageJ. The protein levels were normalized to GAPDH and expressed as the fold change, relative to UT T0, which was set to 1. The densitometry for γH2AX and H2AX was performed across three independent experiments using ImageJ. The protein levels were normalized to Ku70 and expressed as the fold change, relative to UT T0, which was set to 1. (D) Western blotting was performed using antibodies to Rad51 and GAPDH as a loading control. The densitometry for Rad51 was performed across three independent experiments using ImageJ. The protein levels were normalized to GAPDH, and the values were expressed as the fold change, relative to UT T0, which was set to 1. Statistical significance was determined using a Student's *t* test. Error bars represent the mean ± the standard error. *, $P \leq 0.05$; **, $P \leq 0.01$; ns, not significant. Ca, calcium.

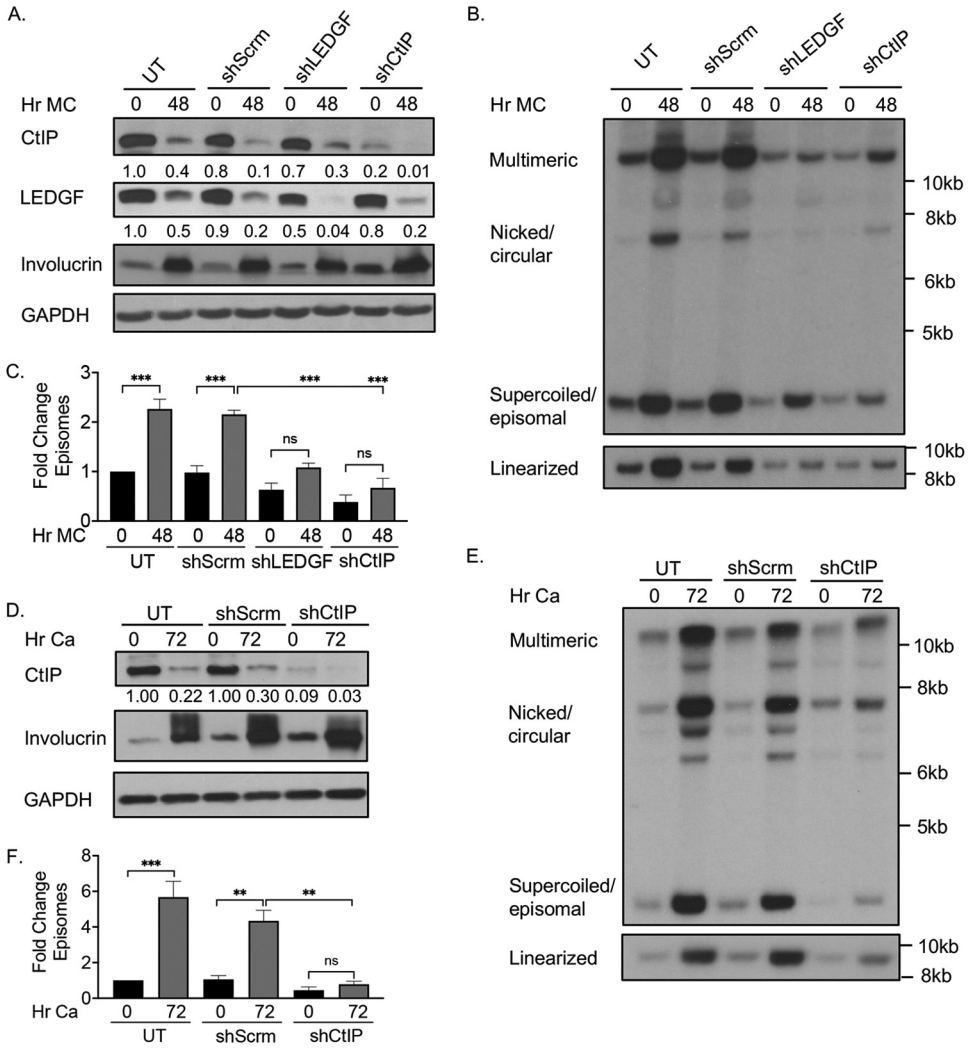

FIG 8 LEDGF and CtIP are required for productive replication. (A–C) CIN612 cells were left untreated (UT) or transiently transduced with either the scramble control shRNA (shScrm), shRNAs to LEDGF (shLEDGF), or CtIP (shCtIP) for 72 h. Cells were harvested as an undifferentiated sample (T0) or induced to differentiate in methylcellulose (MC) for 48 h. Protein and DNA were harvested at the indicated time points. (A) A Western blot analysis was performed using the indicated antibodies, with GAPDH as a loading control. The densitometry for CtIP and LEDGF knockdown was carried out using ImageJ. The protein levels were normalized to GAPDH and expressed as the fold change, relative to the UT T0, which was set to 1. (B) A Southern blot analysis was performed on DNA digested with BamHI (viral DNA noncutter) or HindIII (viral DNA single cutter, linear) to analyze the episomal copy number, using a P^{32}-labeled HPV31 genome as a probe. (C) The densitometry of the episomal bands in panel B across three independent experiments was performed using ImageJ. The values represent the average fold change in episomes, relative to UT T0, which was set to 1. Statistical significance was determined using a one-way analysis of variance (ANOVA). Error bars represent the mean ± the standard error. **, $P \leq 0.01$; ***, $P \leq 0.001$; ns, not significant. (D–F) CIN612 cells were left untreated (UT) or transiently transduced with either the control scramble shRNA (shScrm) or shRNAs to CtIP (shCtIP) for 72 h. Cells were harvested as an undifferentiated sample (T0) or induced to differentiate in high calcium medium for 72 h. (D) A Western blot was performed using antibodies to CtIP, involucrin as differentiation control, and GAPDH as a loading control. The densitometry for CtIP protein levels was carried out using ImageJ. The protein levels were normalized to GAPDH and expressed as the fold change, relative to the undifferentiated untreated sample (UT T0), which was set to 1. (E, F) The Southern blot analysis, densitometry of episomal bands, and statistical analysis were performed as described in panels B and C. Ca, calcium.

linked to the activation of ATM and ATR in response to DSBs and replication stress, respectively, both of which play a critical role in the replication of high-risk HPVs (15, 35, 55). Both ATM and ATR can phosphorylate H2AX to initiate the recruitment of repair factors to sites of damage (56). The ATM signaling pathway is specifically required for viral genome amplification in differentiating cells (11). In contrast, ATR activity is essential for viral replication during both the maintenance and productive phases of the life cycle (12–14). HPV replication in undifferentiated cells occurs in a bidirectional manner that is thought to be

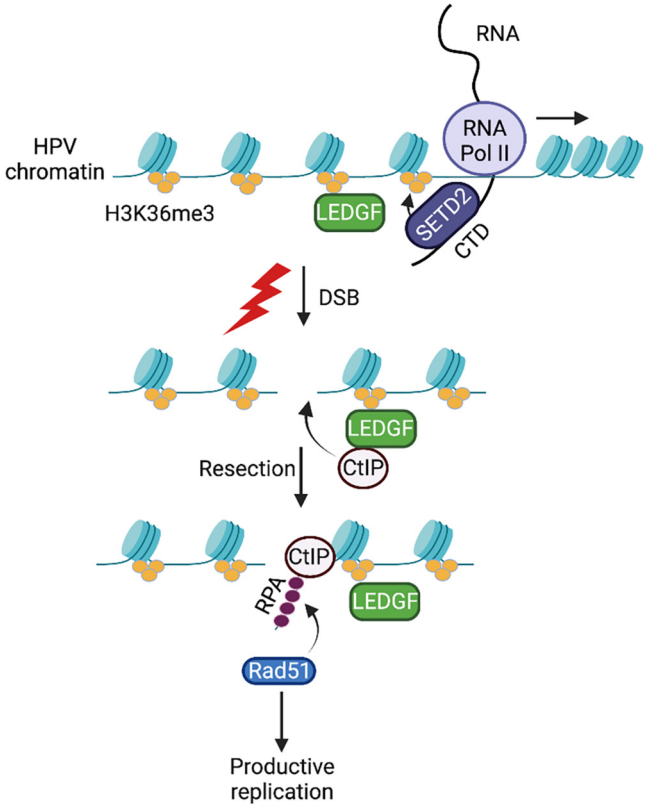

FIG 9 Model for Rad51 recruitment to viral DNA via SETD2-mediated H3K36me3. During the productive phase of the viral life cycle, the SETD2-mediated placement of H3K36me3 on the transcriptionally active viral genes directs the constitutive binding of LEDGF. In response to DNA damage, LEDGF recruits CtIP to viral DNA, which facilitates the resection of double-strand breaks (DSB) and the initiation of HR repair. RPA-coated single-strand DNA is replaced by Rad51, which directs the repair of damaged viral DNA, which, in turn, supports productive viral replication. Created with BioRender.com.

inefficient and to result in stalled replication forks (57). Indeed, components of the ATR response localize to HPV replication foci, indicating that stress occurs on viral DNA during replication (23, 58). A recent study showed that SETD2 promotes ATR activation in response to replication stress through the trimethylation of H3K14 (55). Whether SETD2 deficiency impairs the activation of ATR on viral DNA in undifferentiated cells as well as whether this occurs in an H3K14me3-dependent manner are subjects for future investigations.

Increasing evidence supports a role for chromatin marks that are placed independently of DNA damage in the regulation of HR repair (47). Indeed, SETD2-mediated H3K36me3 plays a critical role in the repair of DSBs in actively transcribed genes (34, 38, 59). Transcription-associated DSBs most commonly occur due to collisions between replication and transcription machinery (60). Epithelial differentiation triggers productive replication as well as the activation of the late promoter, which drives high levels of late genes that facilitate viral genome amplification as well as L1 and L2 to encapsidate newly synthesized viral genomes (20). A recent study from the McBride lab demonstrated that the sites of HPV31 replication and transcription are spatially separated upon differentiation, with replication machinery being located within the cores of the HPV DNA foci and the transcription complexes being localized to the periphery (61). These results suggest that newly synthesized viral genomes are shuttled to the outside of the replication foci to serve as the templates for transcription. The spatial separation of viral transcription and DNA synthesis may serve to protect highly transcribed viral genes from codirectional as well as head-on transcription-replication collisions (TRC) and DNA damage (62). However, our finding that transient transcription inhibition reduces Rad51 recruitment to viral DNA upon differentiation suggests that viral replication, transcription, and DNA repair are linked. SETD2-mediated H3K36me3 is placed during transcription elongation and is required for Rad51 recruitment, further linking transcription to the establishment of the chromatin state

that supports the HR repair of damaged viral DNA. HPV replication is thought to shift from a bidirectional mode in undifferentiated cells to a recombination-dependent, unidirectional mode upon differentiation (63). The transition from bidirectional to unidirectional replication at the onset of differentiation, coupled with the activation of late gene expression, may lead to a significant overlap between active transcription and replication sites, thereby leading to TRCs that render the viral genome susceptible to replication stress and genomic instability (60). How unidirectional replication is coordinated with transcription, and whether this results in an overlap of transcription and replication sites that can result in TRCs, is currently unclear.

Our findings demonstrate a novel role for LEDGF and CtIP in HPV replication, with both DDR factors being required for productive replication upon differentiation. Previous studies demonstrated that LEDGF levels are increased at the protein and mRNA levels in an E6/E7-dependent manner in cervical carcinoma cell lines containing integrated HPV genomes as well as in biopsy specimens of premalignant lesions and cervical cancers (48). LEDGF is overexpressed in numerous human cancers and helps promote cell survival in response to cellular stresses (64–68). LEDGF also plays an important role in HR repair via the recruitment of CtIP (38, 39). Our studies indicate that LEDGF levels are elevated throughout the viral life cycle in cervical and foreskin keratinocytes that stably maintain HPV31 episomes. We have found that LEDGF is bound to viral DNA in a SETD2-dependent and H3K36me3-dependent manner, indicating a direct role in the regulation of viral replication. Interestingly, LEDGF binding increases on viral DNA upon differentiation, despite our previous observation that H3K36me3 enrichment on HPV genomes is similar in undifferentiated and differentiated cells (30). One possibility is that other H3K36me3 effectors are present at higher levels in undifferentiated cells that outcompete LEDGF for binding to viral DNA. Indeed, a recent study showed that a decrease in the levels of the H3K36me3 effector FACT (facilitates chromatin transcription), which is a histone chaperone, allows for the recruitment of LEDGF and its family member HDGF2 to H3K36me2/me3 via their PWWP domains (69). Whether competition occurs between effector proteins for binding to H3K36me3 on viral chromatin and how this changes over the course of the viral life cycle is an interesting avenue for future investigation.

In response to DNA damage, CtIP phosphorylation by ATM and ATR promotes its stable association with chromatin to initiate DSB end resection in conjunction with the Mre11 nuclease as well as through its association with BRCA1 (49, 70, 71). We have found that CtIP is recruited specifically to viral DNA upon differentiation in a SETD2-dependent and H3K36me3-dependent manner as well as that CtIP depletion prevents the recruitment of Rad51 to viral DNA and blocks productive replication. We previously demonstrated that RPA phosphorylated on Ser33, which is a target of ATR and a marker of end resection (72, 73), and localized to sites of HPV31 replication upon differentiation (23). Furthermore, we found that the nuclease activity of Mre11 is required for productive replication (43). These findings, coupled with the CtIP-dependent recruitment of Rad51 to viral DNA, indicate that resection occurs on viral DNA upon differentiation and is necessary for successful viral genome amplification. Interestingly, although SETD2 knockdown and H3K36me3 deficiency resulted in reduced Rad51 recruitment to viral DNA in undifferentiated cells, CtIP depletion had no effect on Rad51 binding. These findings further support an alternative mechanism of SETD2-dependent Rad51 recruitment to viral DNA in undifferentiated cells that is independent of resection. In addition to the methylation of H3K14, SETD2 facilitates the response to replication stress through the recruitment of PALB2 to MRG15-bound H3K36me3 (41). PALB2 physically links BRCA1 and BRCA2 at sites of DNA damage to facilitate the loading of Rad51 onto ssDNA at resected DSBs or stalled replication forks (42). The constitutive tethering of PALB2 to MRG15-H3K36me3 at undamaged chromatin allows a rapid response to DNA stress in active genes by linking BRCA1 and BRCA2 to load Rad51 and facilitate the protection and/or the repair of nearby stressed replication forks (74). Whether the H3K36me3-MRG15-PALB2 axis plays a role in promoting Rad51 recruitment to viral DNA during the maintenance phase of HPV replication is a subject of future studies.

We have found that CtIP protein levels decline drastically upon differentiation, yet CtIP recruitment to viral DNA increases. Previous studies from the Laimins lab showed that cellular DSBs increase in HPV31-positive cells upon differentiation, but HR factors are preferentially recruited to viral DNA (75). The mechanism that regulates this preferential recruitment is currently unknown. However, recent studies showed that high-risk E7 proteins directly interact with the RNF168 ubiquitin ligase, thereby resulting in disrupted repair at cellular DSBs (74). RNF168 is recruited to DSBs in response to ATM signaling and is the rate-limiting factor in the recruitment of DDR proteins to sites of DNA damage (76). In response to DNA damage, RNF168-mediated H2AK15ub recruits 53BP1, which promotes error-prone NHEJ by blocking DSB end resection (77). However, in the S and G_2 phases, RNF168-mediated H2AK15ub at DSB sites promotes HR through the recruitment of BRCA1, which overcomes the anti-resection activity of 53BP1(78). 53BP1 as well as BRCA1 localize to sites of productive replication (23), indicating that RNF168 is active on viral chromatin. RNF168 is required for productive replication; however, the mechanism by which RNF168 contributes to viral replication is currently unclear (74). Our finding that CtIP is recruited to viral DNA suggests that the resection barrier is overcome. One possibility is that the E7-RNF168 interaction serves to direct ubiquitin machinery to damaged viral DNA, thereby providing a mechanism by which the 53BP1 anti-resection barrier can be overcome through the recruitment of BRCA1. DNA damage-induced histone modifications on viral DNA may work in concert with H3K36me3 that is placed during transcription elongation to direct repair to HR and protect viral genome integrity during the productive phase of the viral life cycle.

Although we have uncovered essential roles for LEDGF and CtIP in HPV replication, our findings do not exclude the possibility that other H3K36me3 effectors also contribute to viral replication. Besides HR repair, SETD2 also promotes genome stability through the mismatch repair (MMR) pathway via the binding of H3K36me3 effector MSH6, which is a component of the MMR MutSα complex (79). However, the importance of MMR factors in HPV replication is currently unknown. In addition, the H3K36me3 binding factor DNA methyl transferase 3B (DNMT3B) protects against cryptic transcription initiation by protecting the gene body from the spurious entry of RNAPII (80). SETD2 may protect the fidelity of the initiation of transcription on viral chromatin via DNA methylation through DNMT3B over viral gene bodies. Furthermore, H3K36me3 provides a docking site for the chromatin adapter proteins MRG15 and p52, which subsequently recruit splicing factors (e.g., PTB, SRSF1, and SRSF3) that have been implicated in the splicing of HPV RNAs (81–83). We previously found that SETD2 regulates HPV31 gene expression through the splicing of the L1 RNA and that H3K36me3 peaks over the most commonly used 3′ splice acceptor site (SA3295) that is located at the 3′ end of the E4 open reading frame (30). However, whether H3K36me3 regulates the recruitment of splicing factors to the HPV genome is currently unknown.

Our studies have identified a mechanism by which SETD2-mediated H3K36me3 on viral chromatin epigenetically regulates the HPV31 life cycle through the recruitment of Rad51 via the LEDGF-CtIP pathway. The targeting of deregulated epigenetic pathways is emerging as a promising therapy (84, 85). Understanding how SETD2 regulates the viral life cycle through the binding of alternative H3K36me3 effector proteins to viral chromatin will provide insights regarding the identification of novel therapeutic targets with which to block viral replication for the treatment of HPV-associated diseases. In addition, SETD2 is considered to be a tumor suppressor and is frequently mutated in human cancers (31–33, 86, 87). However, our previous and current studies indicate that high-risk HPVs increase SETD2 protein levels and use SETD2 activity to support the viral life cycle, which may promote viral persistence and genomic instability, which are major risk factors in cancer development.

MATERIALS AND METHODS

Cell culture. Human foreskin keratinocytes (HFKs) were isolated from neonatal foreskin tissue and maintained in DermaLife keratinocyte growth medium (KGM; LifeLine Cell Technology), as previously described (52). HFKs maintaining wild-type HPV31 (HFK-31) were generated as previously described (88). HFK-31 and CIN612 cell lines were cultured in E medium supplemented with 5 ng/mL mouse epidermal

growth factor (EGF, BD Biosciences) in the presence of mitomycin C-treated J2 3T3 fibroblast feeder cells, as previously described (52). J2 fibroblast feeder cells were removed from HPV-positive cells via incubation in Versene (phosphate-buffered saline [PBS] supplemented with 1 mM EDTA) as necessary.

Keratinocyte differentiation. To induce differentiation in methylcellulose, CIN612 cells were suspended in 1.5% methylcellulose, as previously described (52). For high calcium-induced differentiation, subconfluent cells were cultured in serum-free keratinocyte basal medium (KBM, Lonza) containing growth supplements overnight, and they were then changed to KBM media (without supplements) containing 1.5 mM calcium chloride and cultured for 48, 72, or 96 h, as previously described (11). DNA, RNA, and protein were harvested at the indicated time points for further analysis.

Lentivirus production and transduction. Validated lentiviral shRNAs and a scramble nontarget control shRNA were obtained from the UNC-Chapel Hill Lentiviral Core Facility (shSETD2, TRCN0000237837 [30]; shLEDGF, TRCN0000074819 [51]; shCtIP, TRCN0000005403 [50]). The H3.3 and H3.3K36M lentiviral plasmids were kind gifts from David Allis (45). Lentiviral plasmid was cotransfected into 293T cells that were cultured in Dulbecco's modified Eagle's medium (DMEM) supplemented with 10% fetal bovine serum (FBS), along with psPAX2-Gag-Pol-Tet-Env plasmid DNA and pMD2.G-vesicular stomatitis virus G (VSG-G) envelope expressing plasmid DNA using polyethyleneimine (PEI). Supernatants containing lentivirus were harvested at 72 h posttransfection. CIN612 cells were transduced with 5 mL viral supernatant containing 4 μg/mL Polybrene (Sigma). 24 h postransduction, the viral supernatants were replaced with E media, and J2 fibroblast feeder cells were added. The cells were allowed to grow for 48 h and were either harvested as an undifferentiated sample or induced for differentiation.

EU incorporation and immunofluorescence (IF). CIN612 cells were grown on coverslips in the presence of vehicle control (H_2O) or the transcription inhibitor α-amanitin (4 μg/mL) for 17 h prior to harvest, as described previously (89). EU incorporation assays were performed using a Click-iT RNA Alexa Fluor 594 Imaging Kit (ThermoFisher, number C10330), according to the manufacturer's instructions. Briefly, cells were incubated with 1 mM EU for 1 h prior to harvest. At T0 (undifferentiated) and 72 h postcalcium induced differentiation, the cells were washed three times in phosphate-buffered saline (PBS), fixed in 4% paraformaldehyde in PBS for 10 min at room temperature, and then permeabilized in 0.5% Triton X-100-PBS for 10 min at 4°C. Following three PBS washes, the Click-iT reaction was performed for 30 min at room temperature, per the manufacturer's instructions (ThermoFisher). The cells were then washed in PBS and were subsequently blocked in PBS containing 5% bovine serum albumin (BSA) for 1 h at room temperature. The primary antibody to γH2AX(S139) (Cell Signaling, number 2577) was diluted in PBS containing 5% BSA and incubated on coverslips overnight at 4°C. The samples were then washed in PBS and stained with Alexa Fluor 488 anti-rabbit antibody (Invitrogen) for 1 h at room temperature. Cellular DNA was counterstained with 4,6-diamidino-2-phenylindole (DAPI), and the coverslips were mounted in Vectashield (Vector Laboratories). Confocal images were acquired using an LSM 710 confocal laser-scanning microscope (Zeiss) and were processed using the Zeiss Zen software package.

Western blot. Whole-cell lysates were collected by lysing cell pellets in RIPA lysis buffer (50 mM Tris [pH 7.5], 150 mM NaCl, 1 mM EDTA, 1% Nonidet P-40, 0.1% SDS) supplemented with the cOmplete Mini protease inhibitor (Roche) and PhoSTOP phosphatase inhibitor tablets (Roche). For urea solubilization, insoluble cell pellets were resuspended in 8 M urea, 10% β-mercaptoethanol, and 2 mM PMSF, and they were rotated at 37°C for 30 min. An equal amount of protein was electrophoresed using SDS-polyacrylamide gels, and the protein was subsequently transferred to polyvinylidene difluoride (PVDF) membranes (Millipore). The following antibodies were used: SETD2 (a kind gift from Brian Strahl, Epicypher), γH2AX(S139) (Cell Signaling, number 2577), H2AX (Cell Signaling, number 2595), LEDGF (Cell Signaling, number 2088), CtIP (Cell Signaling, number 9201), H3K36me3 (D5A7) (Cell Signaling, number 4909), histone H3 (Cell Signaling, number 3638), Rad51 (Abcam, number ab133534), Nbs1 (Novus Biologicals, number NB100-60654), GAPDH (Santa Cruz, number sc-365062), Ku70 (Santa Cruz, number sc-5309), Involucrin (Santa Cruz, number sc-398952), Loricrin (Novus Biologicals, number NBP1-33610), and Filaggrin (Santa Cruz, number sc-80609). The membranes were then incubated with horseradish peroxidase (HRP)-conjugated secondary antibodies (GE Life Sciences) for 1 h at room temperature. Western blots were developed using the Clarity Western ECL blotting substrate (Bio-Rad). Images were captured using either autoradiography film or a Bio-Rad ChemidocMP imaging system. The images were analyzed using the Bio-Rad ImageLab 6.1 software package. All of the Western blots that are shown are representative images of three independent experiments.

DNA extraction and Southern blot. DNA extraction and Southern blotting were performed as previously described (90). Briefly, cell pellets were resuspended in DNA lysis buffer (400 mM NaCl, 10 mM Tris [pH 7.5], 10 mM EDTA) and incubated with 50 μg/mL RNaseA at room temperature for 15 min. Cell suspensions were then treated with 0.2% SDS and 50 μg/mL proteinase K and were incubated overnight at 37°C. DNA was then extracted using phenol chloroform and precipitated using sodium chloride and ethanol. 3 μg of DNA were digested using BamHI (does not cut the HPV31 genome) or HindIII (linearizes the HPV31 genome) (New England BioLabs). Digested DNA was separated on an 0.8% agarose gel for 18 h at 35 V, transferred to a positively charged nylon membrane (Millipore), and subsequently hybridized to a radioactive DNA probe that consisted of a ^{32}P-labeled linearized HPV31 genome.

Real-time PCR. Total RNA was extracted using RNA Stat 60 (Tel-Test Inc.), and this was followed by DNase digestion (Invitrogen). cDNA was prepared using a Superscript VILO Reverse Transcription Kit (Invitrogen), according to the manufacturer's instructions. qPCR was performed in triplicate using 50 ng of cDNA and an Applied Biosystems QuantStudio 6 Flex real-time PCR thermal cycler (Life Technologies) and SsoAdvanced Universal SYBR Supermix (Bio-Rad). The thermal profile used for the PCR is as follows: 10 min denaturation at 95°C, followed by 40 cycles of 95°C for 15 s and 60°C for 30 s. Melt curves were subsequently performed to ensure proper primer annealing. Relative transcript levels were determined using the threshold cycle method ($2^{-\Delta\Delta CT}$), using GAPDH as an endogenous control gene. The primer sequences are as follows:

LEDGF forward, 5′-CAAGGGAAGAAAGGGCCAAACA-3′; LEDGF reverse, 5′-CGTGCTGGCTTCATGGTTGT-3′; CtIP forward, 5′-AGGGCGAAAGAGAAAAGCGA-3′; CtIP reverse, 5′-TGGACAGGTCAAATACCGCC-3′; GAPDH forward, 5′-CTGTTGCTGTAGCCAAATTCGT-3′; and GAPDH reverse, 5′-ACCCACTCCTCCACCTTTGAC-3′.

Chromatin immunoprecipitation (ChIP). ChIP was performed as previously described (91). Briefly, CIN612 cells were fixed with 1% formaldehyde for 10 min and were then washed three times in ice cold PBS and suspended in collection buffer (100 mM Tris-HCl [pH 9.4], 10 mM DTT supplemented with the COMPLETE protease inhibitor cocktail [Roche]). The cells were subsequently washed with NCP1 buffer (10 mM EDTA, 0.5 mM EGTA, 10 mM HEPES [pH 6.5], 0.25% Triton X-100) and NCP2 buffer (1 mM EDTA, 0.5 mM EGTA, 10 mM HEPES [pH 6.5], 200 mM NaCl) and resuspended in lysis buffer (0.5% Empigen BB, 1% sodium dodecyl sulfate, 10 mM EDTA, 50 mM Tris-HCl [pH 8.0] supplemented with the COMPLETE protease inhibitor cocktail [Roche]). The chromatin was then sonicated for 45 cycles (30 s on, 30 s off) using a Diagenode Bioruptor. The soluble chromatin was incubated overnight at 4°C with 2 μg of antibodies against γH2AX (Millipore, number 05-636-I), LEDGF (Bethyl, number A300-847A), Rad51 (Millipore, number 05-530-I), CtIP (Novus, number NBP1-41205), Nbs1 (Novus, number NB100-60654), or control IgG (Cell Signaling, number 2729) and 20 μL of pre-blocked Dynabeads Protein G (Invitrogen) in IP buffer (1% Triton X-100, 0.1% sodium deoxycholate, 10 mM EDTA, 50 mM Tris-HCl [pH 8.0]). The immune complexes were washed eight times with RIPA buffer (50 mM HEPES [pH 8.0], 1 mM EDTA [pH 8.0], 1% NP-40, 0.7% deoxycholate, 0.5 M LiCl supplemented with protease inhibitor), and this was followed by TE buffer. The complexes were then eluted twice with 50 μL of elution buffer (10 mM Tris [pH 8.0], 1 mM EDTA, 10% SDS) at 65°C for 10 min each. The input samples were purified from 10% of the original lysates. Reverse cross-linking was performed by incubating the samples at 65°C overnight. The samples were then purified using a Qiagen DNA Purification Kit, according to the manufacturer's instructions. The input and immunoprecipitated DNA were subjected to qPCR, as described above, using the following primers to the HPV31 open reading frames or the URR: E1 forward, 5′-ATGTCCATGGGACAGTGGAT-3′; E1 reverse, 5′-CTTTACTATGTCCCTCCAGTCACC-3′; E5 forward, 5′-CGGTCCAAACGCTCTACAA-3′; E5 reverse, 5′-GTACCTGCTGCTTTACATGTTTGA-3′; L1 forward, 5′-CCACCTGTCCCAGTGTCTAAA-3′; L1 reverse, 5′-GCCTGCGTGATAATATATGTTGG-3′; URR forward, 5′-GGCAGGATATAGGGCACGTC-3′; and URR reverse, 5′-GCTGGTGTAGTGGTAGATGCTG-3′. Each independent experiment was performed in a technical triplicate and the data are shown as the means ± the standard deviations of three independent experiments.

ACKNOWLEDGMENTS

We thank David Allis and Brian Strahl for their generous gifts of reagents.

This project was supported by NIH grant R01CA226523 (to C.A.M.), NIH grant P01CA019014 (to C.A.M.), and NIH grant T32AI007419 (to M.M.).

REFERENCES

1. Van Doorslaer K, Tan Q, Xirasagar S, Bandaru S, Gopalan V, Mohamoud Y, Huyen Y, McBride AA. 2013. The Papillomavirus Episteme: a central resource for papillomavirus sequence data and analysis. Nucleic Acids Res 41:D571–D578. https://doi.org/10.1093/nar/gks984.
2. Centers for Disease Control and Prevention (CDC) D of CP and C. 2018. Cancers associated with human papillomavirus, United States, 2011–2015.
3. Ferlay J, Colombet M, Soerjomataram I, Mathers C, Parkin DM, Piñeros M, Znaor A, Bray F. 2019. Estimating the global cancer incidence and mortality in 2018: GLOBOCAN sources and methods. Int J Cancer 144:1941–1953. https://doi.org/10.1002/ijc.31937.
4. You EL, Henry M, Zeitouni AG. 2019. Human papillomavirus–associated oropharyngeal cancer: review of current evidence and management. Curr Oncol 26:119–123. https://doi.org/10.3747/co.26.4819.
5. Pyeon D, Pearce SM, Lank SM, Ahlquist P, Lambert PF. 2009. Establishment of human papillomavirus infection requires cell cycle progression. PLoS Pathog 5:e1000318. https://doi.org/10.1371/journal.ppat.1000318.
6. Hummel M, Hudson JB, Laimins LA. 1992. Differentiation-induced and constitutive transcription of human papillomavirus type 31b in cell lines containing viral episomes. J Virol 66:6070–6080. https://doi.org/10.1128/JVI.66.10.6070-6080.1992.
7. Bienkowska-Haba M, Zwolinska K, Keiffer T, Scott RS, Sapp M. 2023. Human papillomavirus genome copy number is maintained by S-phase amplification, genome loss to the cytosol during mitosis, and degradation in G1 phase. J Virol 97. https://doi.org/10.1128/jvi.01879-22.
8. Bedell MA, Hudson JB, Golub TR, Turyk ME, Hosken M, Wilbanks GD, Laimins LA. 1991. Amplification of human papillomavirus genomes in vitro is dependent on epithelial differentiation. J Virol 65:2254–2260. https://doi.org/10.1128/JVI.65.5.2254-2260.1991.
9. Ozbun MA, Meyers C. 1997. Characterization of late gene transcripts expressed during vegetative replication of human papillomavirus type 31b. J Virol 71:5161–5172. https://doi.org/10.1128/JVI.71.7.5161-5172.1997.
10. Moody C. 2017. Mechanisms by which HPV induces a replication competent environment in differentiating keratinocytes. Viruses 9:261. https://doi.org/10.3390/v9090261.
11. Moody CA, Laimins LA. 2009. Human papillomaviruses activate the ATM DNA damage pathway for viral genome amplification upon differentiation. PLoS Pathog 5:e1000605. https://doi.org/10.1371/journal.ppat.1000605.
12. Anacker DC, Aloor HL, Shepard CN, Lenzi GM, Johnson BA, Kim B, Moody CA. 2016. HPV31 utilizes the ATR-Chk1 pathway to maintain elevated RRM2 levels and a replication-competent environment in differentiating keratinocytes. Virology 499:383–396. https://doi.org/10.1016/j.virol.2016.09.028.
13. Hong S, Cheng S, Iovane A, Laimins LA. 2015. STAT-5 regulates transcription of the topoisomerase IIβ-binding protein 1 (TopBP1) gene to activate the ATR pathway and promote human papillomavirus replication. mBio 6:e02006-15–e02015. https://doi.org/10.1128/mBio.02006-15.
14. Edwards TG, Helmus MJ, Koeller K, Bashkin JK, Fisher C. 2013. Human papillomavirus episome stability is reduced by aphidicolin and controlled by DNA damage response pathways. J Virol 87:3979–3989. https://doi.org/10.1128/JVI.03473-12.
15. Anacker DC, Moody CA. 2017. Modulation of the DNA damage response during the life cycle of human papillomaviruses. Virus Res 231:41–49. https://doi.org/10.1016/j.virusres.2016.11.006.
16. Stünkel W, Bernard HU. 1999. The chromatin structure of the long control region of human papillomavirus type 16 represses viral oncoprotein expression. J Virol 73:1918–1930. https://doi.org/10.1128/JVI.73.3.1918-1930.1999.
17. Favre M, Breitburd F, Croissant O, Orth G. 1977. Chromatin-like structures obtained after alkaline disruption of bovine and human papillomaviruses. J Virol 21:1205–1209. https://doi.org/10.1128/JVI.21.3.1205-1209.1977.
18. You J. 2010. Papillomavirus interaction with cellular chromatin. Biochim Biophys Acta 1799:192–199. https://doi.org/10.1016/j.bbagrm.2009.09.009.
19. Soto D, Song C, McLaughlin-Drubin ME. 2017. Epigenetic alterations in human papillomavirus-associated cancers. Viruses 9:248. https://doi.org/10.3390/v9090248.

20. Mac M, Moody CA. 2020. Epigenetic regulation of the human papillomavirus life cycle. Pathogens 9:483. https://doi.org/10.3390/pathogens9060483.
21. Gautam D, Moody CA. 2016. Impact of the DNA damage response on human papillomavirus chromatin. PLoS Pathog 12:e1005613. https://doi.org/10.1371/journal.ppat.1005613.
22. Burma S, Chen BP, Murphy M, Kurimasa A, Chen DJ. 2001. ATM phosphorylates histone H2AX in response to DNA double-strand breaks. J Biol Chem 276:42462–42467. https://doi.org/10.1074/jbc.C100466200.
23. Gillespie KA, Mehta KP, Laimins LA, Moody CA. 2012. Human papillomaviruses recruit cellular DNA repair and homologous recombination factors to viral replication centers. J Virol 86:9520–9526. https://doi.org/10.1128/JVI.00247-12.
24. Mattiroli F, Vissers JHA, van Dijk WJ, Ikpa P, Citterio E, Vermeulen W, Marteijn JA, Sixma TK. 2012. RNF168 ubiquitinates K13-15 on H2A/H2AX to drive DNA damage signaling. Cell 150:1182–1195. https://doi.org/10.1016/j.cell.2012.08.005.
25. Mailand N, Bekker-Jensen S, Faustrup H, Melander F, Bartek J, Lukas C, Lukas J. 2007. RNF8 ubiquitylates histones at DNA double-strand breaks and promotes assembly of repair proteins. Cell 131:887–900. https://doi.org/10.1016/j.cell.2007.09.040.
26. Uhl M, Csernok A, Aydin S, Kreienberg R, Wiesmüller L, Gatz SA. 2010. Role of SIRT1 in homologous recombination. DNA Repair (Amst) 9:383–393. https://doi.org/10.1016/j.dnarep.2009.12.020.
27. Oberdoerffer P, Michan S, McVay M, Mostoslavsky R, Vann J, Park S-K, Hartlerode A, Stegmuller J, Hafner A, Loerch P, Wright SM, Mills KD, Bonni A, Yankner BA, Scully R, Prolla TA, Alt FW, Sinclair DA. 2008. SIRT1 redistribution on chromatin promotes genomic stability but alters gene expression during aging. Cell 135:907–918. https://doi.org/10.1016/j.cell.2008.10.025.
28. Tang J, Cho NW, Cui G, Manion EM, Shanbhag NM, Botuyan MV, Mer G, Greenberg RA. 2013. Acetylation limits 53BP1 association with damaged chromatin to promote homologous recombination. Nat Struct Mol Biol 20:317–325. https://doi.org/10.1038/nsmb.2499.
29. Hong S, Dutta A, Laimins LA. 2015. The acetyltransferase Tip60 is a critical regulator of the differentiation-dependent amplification of human papillomaviruses. J Virol 89:4668–4675. https://doi.org/10.1128/JVI.03455-14.
30. Gautam D, Johnson BA, Mac M, Moody CA. 2018. SETD2-dependent H3K36me3 plays a critical role in epigenetic regulation of the HPV31 life cycle. PLoS Pathog 14:e1007367. https://doi.org/10.1371/journal.ppat.1007367.
31. Li J, Duns G, Westers H, Sijmons R, van den Berg A, Kok K. 2016. SETD2: an epigenetic modifier with tumor suppressor functionality. Oncotarget 7:50719–50734. https://doi.org/10.18632/oncotarget.9368.
32. Hacker KE, Fahey CC, Shinsky SA, Chiang Y-CJ, DiFiore JV, Jha DK, Vo AH, Shavit JA, Davis IJ, Strahl BD, Rathmell WK. 2016. Structure/function analysis of recurrent mutations in SETD2 protein reveals a critical and conserved role for a SET domain residue in maintaining protein stability and histone H3 Lys-36 trimethylation. J Biol Chem 291:21283–21295. https://doi.org/10.1074/jbc.M116.739375.
33. McDaniel SL, Strahl BD. 2017. Shaping the cellular landscape with Set2/SETD2 methylation. Cell Mol Life Sci 74:3317–3334. https://doi.org/10.1007/s00018-017-2517-x.
34. Pfister SX, Ahrabi S, Zalmas L-P, Sarkar S, Aymard F, Bachrati CZ, Helleday T, Legube G, La Thangue NB, Porter ACG, Humphrey TC. 2014. SETD2-dependent histone H3K36 trimethylation is required for homologous recombination repair and genome stability. Cell Rep 7:2006–2018. https://doi.org/10.1016/j.celrep.2014.05.026.
35. Carvalho S, Vítor AC, Sridhara SC, Martins FB, Raposo AC, Desterro JMP, Ferreira J, de Almeida SF. 2014. SETD2 is required for DNA double-strand break repair and activation of the p53-mediated checkpoint. Elife 3:1–19. https://doi.org/10.7554/eLife.02482.
36. Zhu K, Lei P-J, Ju L-G, Wang X, Huang K, Yang B, Shao C, Zhu Y, Wei G, Fu X-D, Li L, Wu M. 2017. SPOP-containing complex regulates SETD2 stability and H3K36me3-coupled alternative splicing. Nucleic Acids Res 45:92–105. https://doi.org/10.1093/nar/gkw814.
37. Chappell WH, Gautam D, Ok ST, Johnson BA, Anacker DC, Moody CA. 2015. Homologous recombination repair factors Rad51 and BRCA1 are necessary for productive replication of human papillomavirus 31. J Virol 90:2639–2652. https://doi.org/10.1128/JVI.02495-15.
38. Liedtke V, Schröder C, Roggenbuck D, Weiss R, Stohwasser R, Schierack P, Rödiger S, Schenk L. 2021. LEDGF/p75 is required for an efficient DNA damage response. Int J Mol Sci 22:5866. https://doi.org/10.3390/ijms22115866.
39. Daugaard M, Baude A, Fugger K, Povlsen LK, Beck H, Sørensen CS, Petersen NHT, Sorensen PHB, Lukas C, Bartek J, Lukas J, Rohde M, Jäättelä M. 2012. LEDGF (p75) promotes DNA-end resection and homologous recombination. Nat Struct Mol Biol 19:803–810. https://doi.org/10.1038/nsmb.2314.
40. Zhao F, Kim W, Kloeber JA, Lou Z. 2020. DNA end resection and its role in DNA replication and DSB repair choice in mammalian cells. Exp Mol Med 52:1705–1714. https://doi.org/10.1038/s12276-020-00519-1.
41. Bleuyard J-Y, Fournier M, Nakato R, Couturier AM, Katou Y, Ralf C, Hester SS, Dominguez D, Rhodes D, Humphrey TC, Shirahige K, Esashi F. 2017. MRG15-mediated tethering of PALB2 to unperturbed chromatin protects active genes from genotoxic stress. Proc Natl Acad Sci U S A 114:7671–7676. https://doi.org/10.1073/pnas.1620208114.
42. Nepomuceno T, De Gregoriis G, de Oliveira FMB, Suarez-Kurtz G, Monteiro A, Carvalho M. 2017. The role of PALB2 in the DNA damage response and cancer predisposition. Int J Mol Sci 18:1886. https://doi.org/10.3390/ijms18091886.
43. Anacker DC, Gautam D, Gillespie KA, Chappell WH, Moody CA. 2014. Productive replication of human papillomavirus 31 requires DNA repair factor Nbs1. J Virol 88:8528–8544. https://doi.org/10.1128/JVI.00517-14.
44. Kanu N, Grönroos E, Martinez P, Burrell RA, Yi Goh X, Bartkova J, Maya-Mendoza A, Mistrík M, Rowan AJ, Patel H, Rabinowitz A, East P, Wilson G, Santos CR, McGranahan N, Gulati S, Gerlinger M, Birkbak NJ, Joshi T, Alexandrov LB, Stratton MR, Powles T, Matthews N, Bates PA, Stewart A, Szallasi Z, Larkin J, Bartek J, Swanton C. 2015. SETD2 loss-of-function promotes renal cancer branched evolution through replication stress and impaired DNA repair. Oncogene 34:5699–5708. https://doi.org/10.1038/onc.2015.24.
45. Lewis PW, Müller MM, Koletsky MS, Cordero F, Lin S, Banaszynski LA, Garcia BA, Muir TW, Becher OJ, Allis CD. 2013. Inhibition of PRC2 activity by a gain-of-function h3 mutation found in pediatric glioblastoma. Science 340:857–861. https://doi.org/10.1126/science.1232245.
46. Marnef A, Cohen S, Legube G. 2017. Transcription-coupled DNA double-strand break repair: active genes need special care. J Mol Biol 429:1277–1288. https://doi.org/10.1016/j.jmb.2017.03.024.
47. Chen Z, Tyler JK. 2022. The chromatin landscape channels DNA double-strand breaks to distinct repair pathways. Front Cell Dev Biol 10:1–18. https://doi.org/10.3389/fcell.2022.909696.
48. Leitz J, Reuschenbach M, Lohrey C, Honegger A, Accardi R, Tommasino M, Llano M, von Knebel Doeberitz M, Hoppe-Seyler K, Hoppe-Seyler F. 2014. Oncogenic human papillomaviruses activate the tumor-associated lens epithelial-derived growth factor (LEDGF) gene. PLoS Pathog 10:e1003957. https://doi.org/10.1371/journal.ppat.1003957.
49. Mozaffari NL, Pagliarulo F, Sartori AA. 2021. Human CtIP: a 'double agent' in DNA repair and tumorigenesis. Semin Cell Dev Biol 113:47–56. https://doi.org/10.1016/j.semcdb.2020.09.001.
50. Abdisalaam S, Mukherjee S, Bhattacharya S, Kumari S, Sinha D, Ortega J, Li G-M, Sadek HA, Krishnan S, Asaithamby A. 2022. NBS1-CtIP–mediated DNA end resection suppresses cGAS binding to micronuclei. Nucleic Acids Res 50:2681–2699. https://doi.org/10.1093/nar/gkac079.
51. Gupta K, Brady T, Dyer BM, Malani N, Hwang Y, Male F, Nolte RT, Wang L, Velthuisen E, Jeffrey J, Van Duyne GD, Bushman FD. 2014. Allosteric inhibition of human immunodeficiency virus integrase. J Biol Chem 289:20477–20488. https://doi.org/10.1074/jbc.M114.551119.
52. Wilson R, Laimins LA. 2005. Differentiation of HPV-containing cells using organotypic "raft" culture or methylcellulose, p 157–170. *In* Human Papillomaviruses. Humana Press, New Jersey.
53. Wang H-K, Duffy AA, Broker TR, Chow LT. 2009. Robust production and passaging of infectious HPV in squamous epithelium of primary human keratinocytes. Genes Dev 23:181–194. https://doi.org/10.1101/gad.1735109.
54. Kousholt AN, Fugger K, Hoffmann S, Larsen BD, Menzel T, Sartori AA, Sørensen CS. 2012. CtIP-dependent DNA resection is required for DNA damage checkpoint maintenance but not initiation. J Cell Biol 197:869–876. https://doi.org/10.1083/jcb.201111065.
55. Zhu Q, Yang Q, Lu X, Wang H, Tong L, Li Z, Liu G, Bao Y, Xu X, Gu L, Yuan J, Liu X, Zhu WG. 2021. SETD2-mediated H3K14 trimethylation promotes ATR activation and stalled replication fork restart in response to DNA replication stress. Proc Natl Acad Sci U S A 118:2011278118.
56. Blackford AN, Jackson SP. 2017. ATM, ATR, and DNA-PK: the trinity at the heart of the DNA damage response. Mol Cell 66:801–817. https://doi.org/10.1016/j.molcel.2017.05.015.
57. Liblekas L, Piirsoo A, Laanemets A, Tombak E-M, Laaneväli A, Ustav E, Ustav M, Piirsoo M. 2021. Analysis of the replication mechanisms of the human papillomavirus genomes. Front Microbiol 12. https://doi.org/10.3389/fmicb.2021.738125.
58. Reinson T, Toots M, Kadaja M, Pipitch R, Allik M, Ustav E, Ustav M. 2013. Engagement of the ATR-dependent DNA damage response at the human papillomavirus 18 replication centers during the initial amplification. J Virol 87:951–964. https://doi.org/10.1128/JVI.01943-12.

59. Aymard F, Bugler B, Schmidt CK, Guillou E, Caron P, Briois S, Iacovoni JS, Daburon V, Miller KM, Jackson SP, Legube G. 2014. Transcriptionally active chromatin recruits homologous recombination at DNA double-strand breaks. Nat Struct Mol Biol 21:366–374. https://doi.org/10.1038/nsmb.2796.
60. Hamperl S, Cimprich KA. 2016. Conflict resolution in the genome: how transcription and replication make it work. Cell 167:1455–1467. https://doi.org/10.1016/j.cell.2016.09.053.
61. Khurana S, Markowitz TE, Kabat J, McBride AA. 2021. Spatial and functional organization of human papillomavirus replication foci in the productive stage of infection. mBio 12:e02684-21. https://doi.org/10.1128/mBio.02684-21.
62. Lalonde M, Trauner M, Werner M, Hamperl S. 2021. Consequences and resolution of transcription–replication conflicts. Life 11:637. https://doi.org/10.3390/life11070637.
63. Flores ER, Lambert PF. 1997. Evidence for a switch in the mode of human papillomavirus type 16 DNA replication during the viral life cycle. J Virol 71:7167–7179. https://doi.org/10.1128/JVI.71.10.7167-7179.1997.
64. Daniels T, Zhang J, Gutierrez I, Elliot ML, Yamada B, Heeb MJ, Sheets SM, Wu X, Casiano CA. 2005. Antinuclear autoantibodies in prostate cancer: immunity to LEDGF/p75, a survival protein highly expressed in prostate tumors and cleaved during apoptosis. Prostate 62:14–26. https://doi.org/10.1002/pros.20112.
65. Daugaard M, Kirkegaard-Sørensen T, Ostenfeld MS, Aaboe M, Høyer-Hansen M, Orntoft TF, Rohde M, Jäättelä M. 2007. Lens epithelium-derived growth factor is an Hsp70-2 regulated guardian of lysosomal stability in human cancer. Cancer Res 67:2559–2567. https://doi.org/10.1158/0008-5472.CAN-06-4121.
66. Basu A, Rojas H, Banerjee H, Cabrera IB, Perez KY, De León M, Casiano CA. 2012. Expression of the stress response oncoprotein LEDGF/p75 in human cancer: a study of 21 tumor types. PLoS One 7:e30132. https://doi.org/10.1371/journal.pone.0030132.
67. Cohen B, Addadi Y, Sapoznik S, Meir G, Kalchenko V, Harmelin A, Ben-Dor S, Neeman M. 2009. Transcriptional regulation of vascular endothelial growth factor C by oxidative and thermal stress is mediated by lens epithelium-derived growth factor/p75. Neoplasia 11:921–933. https://doi.org/10.1593/neo.09636.
68. Bhargavan B, Fatma N, Chhunchha B, Singh V, Kubo E, Singh DP. 2012. LEDGF gene silencing impairs the tumorigenicity of prostate cancer DU145 cells by abating the expression of Hsp27 and activation of the Akt/ERK signaling pathway. Cell Death Dis 3:e316. https://doi.org/10.1038/cddis.2012.57.
69. LeRoy G, Oksuz O, Descostes N, Aoi Y, Ganai RA, Kara HO, Yu JR, Lee CH, Stafford J, Shilatifard A, Reinberg D. 2019. LEDGF and HDGF2 relieve the nucleosome-induced barrier to transcription in differentiated cells. Sci Adv 5:1–13. https://doi.org/10.1126/sciadv.aay3068.
70. Wang H, Shi LZ, Wong CCL, Han X, Hwang PY-H, Truong LN, Zhu Q, Shao Z, Chen DJ, Berns MW, Yates JR, Chen L, Wu X. 2013. The interaction of CtIP and Nbs1 connects CDK and ATM to regulate HR–mediated double-strand break repair. PLoS Genet 9:e1003277. https://doi.org/10.1371/journal.pgen.1003277.
71. Peterson SE, Li Y, Wu-Baer F, Chait BT, Baer R, Yan H, Gottesman ME, Gautier J. 2013. Activation of DSB processing requires phosphorylation of CtIP by ATR. Mol Cell 49:657–667. https://doi.org/10.1016/j.molcel.2012.11.020.
72. Bunting SF, Callén E, Wong N, Chen H-T, Polato F, Gunn A, Bothmer A, Feldhahn N, Fernandez-Capetillo O, Cao L, Xu X, Deng C-X, Finkel T, Nussenzweig M, Stark JM, Nussenzweig A. 2010. 53BP1 inhibits homologous recombination in Brca1-deficient cells by blocking resection of DNA breaks. Cell 141:243–254. https://doi.org/10.1016/j.cell.2010.03.012.
73. Liu S, Opiyo SO, Manthey K, Glanzer JG, Ashley AK, Amerin C, Troksa K, Shrivastav M, Nickoloff JA, Oakley GG. 2012. Distinct roles for DNA-PK, ATM and ATR in RPA phosphorylation and checkpoint activation in response to replication stress. Nucleic Acids Res 40:10780–10794. https://doi.org/10.1093/nar/gks849.
74. Sitz J, Blanchet SA, Gameiro SF, Biquand E, Morgan TM, Galloy M, Dessapt J, Lavoie EG, Blondeau A, Smith BC, Mymryk JS, Moody CA, Fradet-Turcotte A. 2019. Human papillomavirus E7 oncoprotein targets RNF168 to hijack the host DNA damage response. Proc Natl Acad Sci U S A 116:19552–19562. https://doi.org/10.1073/pnas.1906102116.
75. Mehta K, Laimins L. 2018. Human papillomaviruses preferentially recruit DNA repair factors to viral genomes for rapid repair and amplification. mBio 9:e00064-18. https://doi.org/10.1128/mBio.00064-18.
76. Gudjonsson T, Altmeyer M, Savic V, Toledo L, Dinant C, Grøfte M, Bartkova J, Poulsen M, Oka Y, Bekker-Jensen S, Mailand N, Neumann B, Heriche J-K, Shearer R, Saunders D, Bartek J, Lukas J, Lukas C. 2012. TRIP12 and UBR5 suppress spreading of chromatin ubiquitylation at damaged chromosomes. Cell 150:697–709. https://doi.org/10.1016/j.cell.2012.06.039.
77. Kelliher J, Ghosal G, Leung JWC. 2022. New answers to the old RIDDLE: RNF168 and the DNA damage response pathway. FEBS J 289:2467–2480. https://doi.org/10.1111/febs.15857.
78. Becker JR, Clifford G, Bonnet C, Groth A, Wilson MD, Chapman JR. 2021. BARD1 reads H2A lysine 15 ubiquitination to direct homologous recombination. Nature 596:433–437. https://doi.org/10.1038/s41586-021-03776-w.
79. Li F, Mao G, Tong D, Huang J, Gu L, Yang W, Li G-M. 2013. The histone mark H3K36me3 regulates human DNA mismatch repair through its interaction with MutSα. Cell 153:590–600. https://doi.org/10.1016/j.cell.2013.03.025.
80. Neri F, Rapelli S, Krepelova A, Incarnato D, Parlato C, Basile G, Maldotti M, Anselmi F, Oliviero S. 2017. Intragenic DNA methylation prevents spurious transcription initiation. Nature 543:72–77. https://doi.org/10.1038/nature21373.
81. Luco RF, Pan Q, Tominaga K, Blencowe BJ, Pereira-Smith OM, Misteli T. 2010. Regulation of alternative splicing by histone modifications. Science 327:996–1000. https://doi.org/10.1126/science.1184208.
82. Graham SV, Faizo AAA. 2017. Control of human papillomavirus gene expression by alternative splicing. Virus Res 231:83–95. https://doi.org/10.1016/j.virusres.2016.11.016.
83. Pradeepa MM, Sutherland HG, Ule J, Grimes GR, Bickmore WA. 2012. Psip1/Ledgf p52 binds methylated histone H3K36 and splicing factors and contributes to the regulation of alternative splicing. PLoS Genet 8:e1002717. https://doi.org/10.1371/journal.pgen.1002717.
84. Cheng Y, He C, Wang M, Ma X, Mo F, Yang S, Han J, Wei X. 2019. Targeting epigenetic regulators for cancer therapy: mechanisms and advances in clinical trials. Signal Transduct Target Ther 4:62. https://doi.org/10.1038/s41392-019-0095-0.
85. Lu Y, Chan Y-T, Tan H-Y, Li S, Wang N, Feng Y. 2020. Epigenetic regulation in human cancer: the potential role of epi-drug in cancer therapy. Mol Cancer 19:79. https://doi.org/10.1186/s12943-020-01197-3.
86. Fahey CC, Davis IJ. 2017. SETting the stage for cancer development: SETD2 and the consequences of lost methylation. Cold Spring Harb Perspect Med 7:a026468. https://doi.org/10.1101/cshperspect.a026468.
87. Lawrence MS, Stojanov P, Mermel CH, Robinson JT, Garraway LA, Golub TR, Meyerson M, Gabriel SB, Lander ES, Getz G. 2014. Discovery and saturation analysis of cancer genes across 21 tumour types. Nature 505:495–501. https://doi.org/10.1038/nature12912.
88. Longworth MS, Laimins LA. 2004. The binding of histone deacetylases and the integrity of zinc finger-like motifs of the E7 protein are essential for the life cycle of human papillomavirus type 31. J Virol 78:3533–3541. https://doi.org/10.1128/jvi.78.7.3533-3541.2004.
89. Kotsantis P, Silva LM, Irmscher S, Jones RM, Folkes L, Gromak N, Petermann E. 2016. Increased global transcription activity as a mechanism of replication stress in cancer. Nat Commun 7:13087. https://doi.org/10.1038/ncomms13087.
90. Thomas JT, Hubert WG, Ruesch MN, Laimins LA. 1999. Human papillomavirus type 31 oncoproteins E6 and E7 are required for the maintenance of episomes during the viral life cycle in normal human keratinocytes. Proc Natl Acad Sci U S A 96:8449–8454. https://doi.org/10.1073/pnas.96.15.8449.
91. Wong P-P, Pickard A, McCance DJ. 2010. p300 alters keratinocyte cell growth and differentiation through regulation of p21Waf1/CIP1. PLoS One 5:e8369. https://doi.org/10.1371/journal.pone.0008369.